A review of carbon material-based Z-scheme and S-scheme heterojunctions for photocatalytic clean energy generation

Sahil Rana[1], Amit Kumar[1,*], WANG Tong-tong[2], Gaurav Sharma[1], Pooja Dhiman[1], Alberto García-Penas[3]

（1. *International Research Centre of Nanotechnology for Himalayan Sustainability (IRCNHS)*, *Shoolini University*, *Solan*, 173229, *India*;
2. *Interdisciplinary and Innovate Research*, *Xi'an University of Architecture and Technology*, *Xi'an*, 710055, *China*;
3. *Departamento de Ciencia e Ingeniería de Materiales e Ingeniería Química (IAAB)*, *Universidad Carlos III de Madrid*, *Legan'es*, 28911, *Spain*）

Abstract： Carbon materials, including carbon nanotubes/nanofibers, graphene, graphene oxide, reduced graphene oxide, graphyne, graphdiyne, carbon quantum dots and fullerenes, have received considerable attention in recent years because of their unique properties such as high conductivity, excellent stability and biocompatibility. The integration of these materials into Z-scheme and S-scheme heterojunctions has emerged as a transformative strategy to increase their photocatalytic efficiency for energy conversion applications. We first consider the fundamental principles of clean energy generation such as photocatalytic H_2 generation and CO_2 reduction, elucidating their respective mechanisms and advantages. Various types of carbon materials, their synthesis and construction of Z-scheme and S-scheme heterojunctions are then discussed, emphasizing their role in promoting charge separation, reducing recombination losses and extending the spectral response range. With a focus on solar energy production, recent advances in carbon-based Z-scheme and S-scheme heterojunctions are discussed and summarized for photocatalytic H_2 generation and CO_2 reduction. Lastly, the current problems in the field of carbon-based photocatalysts are discussed with insights for the future development of this field.

Key words: Carbonaceous; Heterojunctions; Z-scheme; S-scheme; Photocatalysis; Hydrogen materials

1 Introduction

One of the most pressing problems facing humanity today is the worldwide shortage of energy. Because of the overuse and exploitation of readily available fossil fuels, non-renewable energy supplies like coal and petroleum may eventually run out, raising concerns about the use and exploitation of clean, viable sources of energy. For near and foreseeable future, solar energy remains the most plausible source of renewable power[1]. One of the most promising approaches is the establishment of new energy systems that transform sunlight into photoelectrical and chemical energy. Examples of these systems include the production of hydrogen (H_2) through water splitting and the photocatalytic reduction of carbon dioxide (CO_2) to chemical fuels[2,3]. Under ambient settings, converting atmospheric CO_2 and H_2O into fuels like methanol, methane and carbon monoxide has proven to be a sustainable option without further harming the environment[4]. Photocatalysis is a green technique for transforming solar energy into chemical energy, which accelerate any chemical reaction by lowering the activation energy required for the reaction to proceed by direct or catalytic photon illumination[5]. It is an advanced oxidation process that uses photons' active and passive involvement to split water and reduce carbon dioxide amidst the UV-visible radiation to produce hydrogen and solar fuels respectively[6]. This process is important because the process has low secondary pollution, gentle reaction conditions, excellent efficiency, fast speed and no selectivity. Actually, photocatalysis is seen to be among the best strategies available to help solve the world's energy and environmental problems. Through the application of this technology, we can lessen our reliance on non-renewable energy sources and enhance the environment for coming generations[7].

A rapidly developing class of materials, known as carbon materials, can be found in zero-dimensional

Received date: 2024-02-01； **Revised date:** 2024-04-26
Corresponding author: Amit Kumar. E-mail: mittuchem83@gmail.com

to three-dimensional arrangements. Examples of these materials include carbon nanotubes (CNTs), carbon nanofibers (CNFs), carbon quantum dots (CQDs), graphene, graphene oxide (GO), reduced graphene oxide (rGO), graphyne (GY), graphdiyne (GDY), fullerenes and carbon sponge/aerogel[8–11]. Besides these materials, carbon nitride is also a reliable and versatile photocatalyst for a number of photocatalytic applications[12,13]. Their remarkable electrical, thermal, mechanical and optical qualities have drawn a lot of interest. These structures have excellent physicochemical stability, strong mechanical strength, excellent electrical conductivity, better charge transport pathways, enormous surface area and capability for the carbon atoms to exist in sp, sp^2 and sp^3 hybridization states[14,15]. Carbon-based materials exhibit numerous benefits including affordability, abundance of resources, minimal environmental toxicity, extended durability and resistance to acid/base corrosion[16]. As a result, carbon materials of this kind have found many important uses, especially in photocatalysis. This clean, eco-friendly, viable, economical and renewable process uses light as its source to ignite catalysts for chemical processes[17]. The photocatalytic carbon materials' framework, surface area, atomic layer density and band gap energy have a significant influence on their capacity to capture light and the paths by which charges migrate through them[18]. The doped porous carbon materials have also been used as robust catalysts for CO_2 reduction[19]. Carbon materials are appealing for a variety of photocatalytic applications because of band gap's flexibility. As such, excellent photocatalytic effectiveness of these materials can be used for the clean energy generation[20].

As is well known, quick electron-hole recombination and poor light usage dramatically reduce overall photocatalytic performance[21]. Special methodologies are necessary to build optimal photocatalysts that decrease electron-hole recombination while retaining their reducing and oxidizing abilities. Heterojunction construction has emerged as one of the most promising techniques, offering advantages such as increased light harvesting, delayed electron-hole recombination and rapid charge transfer[22]. The carbon materials can form various types of heterojunctions such as type-II, p-n, Z-scheme and S-scheme, with other materials and semiconductors for a number of energy related applications[23–26]. In comparison to other noble metals, their inexpensive cost of manufacture and excellent electron transfer capabilities make them a superior candidate as electron mediators in semiconductor heterojunctions[27]. Among various heterojunction types, the Z-scheme and S-scheme heterojunctions have gathered much attention recently in the carbonaceous based photocatalysts for energy conversion purposes[28,29]. Although the traditional heterojunctions appears to improve charge transmission in space, it diminishes the redox capability of the photocarriers produced in photocatalytic heterojunction setup[30].

The present review explores and summarizes the recent advancements in the applications of carbon materials based Z-scheme and S-scheme heterojunction photocatalysts for H_2 energy generation and CO_2 reduction. The photocatalytic H_2 evolution and CO_2 reduction mechanisms are briefly discussed and the charge transfer mechanisms in Z-scheme and S-scheme heterojunctions are also explored. Different types of carbon materials, their synthetic routes and their role and properties as a photocatalyst are comprehensively addressed. Finally, according to current state of knowledge, the bottlenecks, challenges and future perspectives are proposed.

2 Photocatalysis

2.1 Photocatalytic clean energy generation-fundamentals and mechanisms

Deemed as a "free" renewable energy source with negligible environmental effects, solar radiation is becoming more and more important in addressing the fundamental issues related to energy and the environment[31]. Solar-powered photocatalysis is thought to be a useful method for converting solar energy and offers a possible remedy for the world's energy and environmental problems[32]. Photocatalytic reactions can reduce energy problems by conversion of solar energy into clean chemical energy that can be easily

transported, stored and used[33]. Photocatalytic H_2 generation and CO_2 reduction are popular processes used to transform renewable solar energy into chemical energy. The procedure is based on the ideas of charge separation in which reactions include excited electrons and holes[34].

2.1.1 H_2 generation

As an alternative form of energy, hydrogen is an excellent replacement for different fossil fuels and can assist address the growing challenges of energy crisis[35]. The production of hydrogen through photocatalysis is a thermodynamically ascending reaction, possessing a Gibbs free energy of 1.23 eV or 237 kJ/mol. As a result, the semiconductor employed for photocatalysis should have band gap energy of 1.23 to 3 eV[36]. Moreover, the valence band (VB) and conduction band (CB) locations should be suitable for photocatalytic water splitting, with the CB edge being more negative than $E^0(H_2/H_2O)$ = 0 V vs. NHE and the VB edge being more positive than $E^0(O_2/H_2O)$ = 1.23 V vs. NHE[37]. Generally, there are 3 easy steps to understand the hydrogen evolution approach by water splitting. (1) Photon absorption results in the formation of electron-hole pairs. (2) The separation and movement of previously created electrons and holes constitute. (3) Holes on the photocatalyst's VB oxidize water molecules to oxygen while protons on CB are converted to hydrogen by electrons[38]. Electrons flow from the VB into CB when the holes remain there. Both these light-driven electrons and holes have the ability to reduce H^+ and oxidize H_2O, respectively, if the lower edge of the CB is positioned at a greater negative potential relative to the H^+ to H_2 reduction potential (0 V vs. NHE). Additionally, a greater VB peak is required in comparison to the $H_2O \rightarrow O_2$ oxidation potential (1.23 V vs. NHE)[39]. The following equations contain the redox processes that occur during the photocatalytic generation of hydrogen[40] and schematic illustration of the mechanism is shown in Fig. 1a.

Oxidation: $2H_2O \rightarrow O_2 + 4H^+ + 4e^-$ $E^0 = 1.23$ eV

Reduction: $2H^+ + 2e^- \rightarrow H_2$ $E^0 = 0.0$ eV

Overall: $2H_2O \rightarrow O_2 + 2H_2$ $E^0 = -1.23$ eV

2.1.2 CO_2 reduction

Since it uses no additional energy and has no negative impacts on the environment, photocatalytic CO_2 reduction is a very effective technique. A vast array of compounds such as CO, CH_4, HCOOH, CH_3OH, C_2H_5OH and HCHO are formed from CO_2 by obtaining different amounts of protons and electrons[38]. A redox reaction combining the photocatalytic reduction of CO_2 and the oxidation of water produces solar fuel. The photocatalyst's VB and CB are commonly utilized to explain the principles of CO_2 reduction mechanism. The possibility that solar fuel will be produced is determined by the photocatalyst's CB position[41,42]. The following steps should be followed in general while performing the photocatalytic CO_2 reduction process. The electrons of the photocatalyst are activated and transferred from its VB to CB so as to form light-driven particles. In order to initiate a photocatalytic reaction, the photo-induced charges will either split and travel to the photocatalyst's exterior or they can reunite to generate heat or

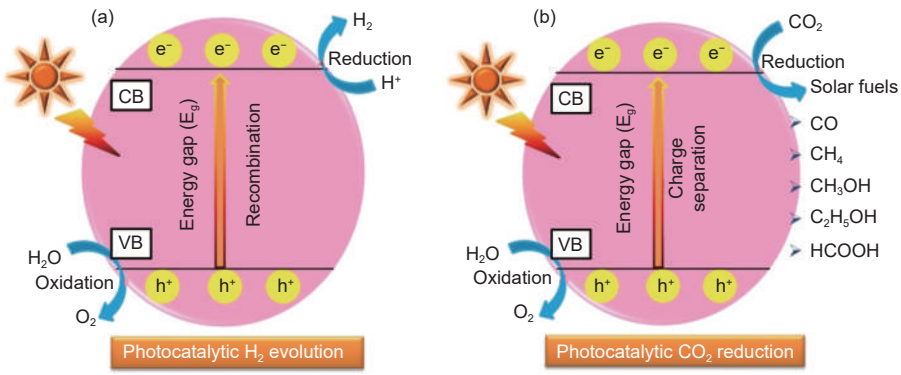

Fig. 1 Schematic illustration of (a) photocatalytic H_2 generation and (b) photocatalytic CO_2 reduction mechanism

photons. There is also low-level CO_2 absorption by the catalysts. The photo-induced electrons on the surface of photocatalysts transform CO_2 into fuels[43]. A higher negative conductive potential than the required standard potential and effective electron transporting to the exterior of semiconductor, where CO_2 is adsorbed, are indicators of the efficacy of CO_2 reduction. Thus, for highly-efficient photocatalytic CO_2 reduction, an ideal photocatalyst with appropriate band configuration, increased visible light utilization and improved CO_2 activation efficiency is required[44]. Eqs. below depict the overall framework of reactions for photocatalytic reduction of CO_2 into different fuels[41] and Fig. 1b shows a graphical illustration of this scheme.

$$CO_2 + 2H^+ + 2e^- \rightarrow HCOOH \qquad E^0 = -0.61\ V$$

$$CO_2 + 2H^+ + 2e^- \rightarrow CO + H_2O \qquad E^0 = -0.53\ V$$

$$CO_2 + 4H^+ + 4e^- \rightarrow HCHO + H_2O \qquad E^0 = -0.48\ V$$

$$CO_2 + 6H^+ + 6e^- \rightarrow CH_3OH + H_2O \qquad E^0 = -0.38\ V$$

$$CO_2 + 8H^+ + 8e^- \rightarrow CH_4 + 2H_2O \qquad E^0 = -0.24\ V$$

$$2CO_2 + 12H^+ + 12e^- \rightarrow C_2H_5OH + 3H_2O \qquad E^0 = -0.33\ V$$

2.2 Heterojunctions based photocatalysis-fundamentals and mechanisms

The result of the hybridization of two semiconductors with different energy gaps and electrical configurations is a heterojunction or a junction interface[45]. When a sufficient light source is present, electron-hole (e^--h^+) pairs arise on the exteriors of 2 combining semiconductors. For photocatalysts, recombination of these e^--h^+ pairs is a major problem. However, two semiconductors work together to reduce recombination impacts in a heterojunction[46]. Consequently, the inherent shortcomings of single photocatalysts are addressed by heterojunction photocatalysis. The main advantages of establishing the heterojunctions are below: The capacity of heterojunctions to raise the wavelength at which light is absorbed, greater distances separating electron-hole pairs and an increase in catalytic efficiency brought about by the substitution of another semiconductor. A higher separation rate and appropriate association of materials based on semiconductors cause charge carriers to move within the heterojunctions[47–49]. Heterojunctions in photocatalysis are classified into traditional and non-traditional types with the traditional ones constituting type-I or straddling type, type-II or staggered gap and type-III or broken gap heterojunctions. On the other hand, non-traditional includes p-n, Z-scheme, S-scheme and Schottky junction[41]. There are different charge carrier separation procedures for different systems. Here, in this review, we will discuss the Z-scheme and S-scheme heterojunctions only.

2.2.1 Z-scheme

The separation of light-induced carriers can be facilitated by conventional heterojunctions. However, at the same time, the composites' VB and CB potential for the light-induced holes and electrons, respectively, are inexorably decreased, which is detrimental to the production of active radicals. Researchers have created the Z-scheme heterojunction photocatalytic system to address this issue which was motivated by the photochemical reaction of plant light collaboration in nature. This heterojunction framework is known as Z-scheme heterojunction because its electron transport mechanism is akin to the English letter Z[50]. The Z-scheme heterojunctions can be divided into 3 different types namely traditional Z-scheme heterojunction, all-solid-state Z-scheme heterojunction and direct Z-scheme heterojunction[51]. A suitable shuttle redox ion mediator is used to pair 2 distinct photocatalysts for a conventional Z-scheme as shown in Fig. 2a. The light-induced holes in the VB of photocatalyst (PC) 1 are devoured by the electron donor species, whereas the light-induced electrons in the CB of PC 2 are absorbed by the electron acceptor species when the photocatalysts are subjected to light. The electrons inPC 1's CB having high redox power and the light-driven holes in PC 2's VB are both conserved and can take part in reduction and oxidation reactions, respectively[52]. This system has several drawbacks such as side reactions and its compatibility in solution phase only[53]. In an all-solid-state Z-scheme charge-transfer pathway, light-induced electrons in PC 2's CB move to the robust conductor and then to PC 1's VB following each photocatalyst's activation un-

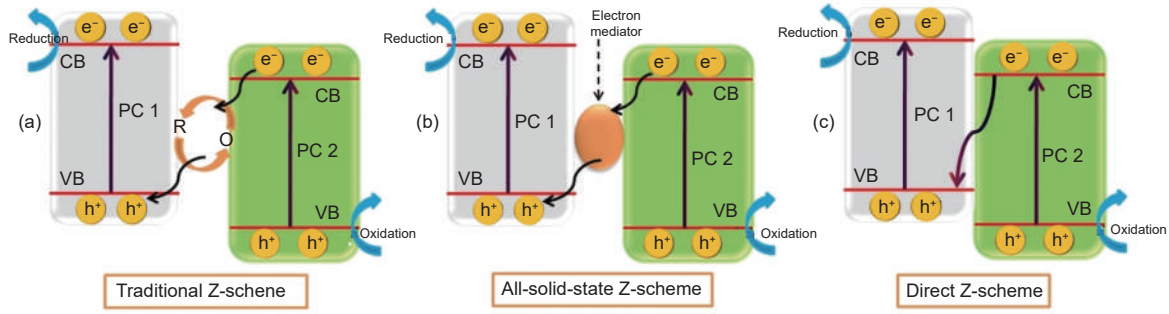

Fig. 2 Schematic illustration of (a) traditional Z-scheme, (b) all-solid-state Z-scheme and (c) direct Z-scheme heterojunction

der irradiation (Fig. 2b). This system works in both liquid and gas environments because it uses a solid conductor rather than shuttle redox ion pairs. Moreover, it has a much shorter charge-transfer length, which can dramatically speed up charge transfer[54]. Due to their reliance on conductors for charge transfer, all-solid-state Z-scheme heterojunctions are not satisfying. In direct Z-scheme heterojunction, charge transfer mediator is not used[55]. Recombination takes place in a direct Z-scheme system between the holes from the semiconductor having less positive VB and the weak electrons from the semiconductor having less negative CB as visible from Fig. 2c[56]. Thus, the Z-scheme system's overall redox potential increases because the holes having strong oxidation capability and the electrons having excellent reduction capability cannot recombine and be constantly maintained for additional photocatalytic processes. By eliminating unnecessary electrons and holes and maintaining the system's high redox potential, Z-scheme heterojunction offers a novel strategy for increasing photocatalyst activity[57].

2.2.2 S-scheme

Z-scheme heterojunctions have significant drawbacks, so a novel idea was required to provide a vivid and concise explanation of the photocatalytic operation[53]. Step-scheme systems, which resemble type-II heterojunction except for the significantly different method of charge migration, are demonstrated between two n-type semiconductors having staggered band structures[57]. The charge transfer pathway in the S-scheme heterojunction can be explained as the combination of three factors namely internal electric field, band bending and columbic interaction[58]. These factors mainly behave as the driving forces for recombination of holes in VB of oxidation photocatalyst (OP) and electrons in CB of reduction photocatalyst (RP)[59]. As a result, the valuable light-induced electrons in the CB of RP and the holes in the VB of OP are retained to participate in photocatalytic processes, while the worthless electrons and holes are removed through recombination[60]. Along the interface of RP and OP, there are electron depletion and aggregation layers formed by the spontaneous diffusion of electrons from RP to OP when these 2 semiconductors are in close proximity to one other. Whereas the RP is positively charged, the OP is negatively charged. There is concurrent formation of an internal electric field that directs from RP to OP. Light-driven electrons move from OP to RP more quickly because of this internal electric field. OP and RP should have identical Fermi energies when they come into interaction. As a result, the Fermi levels of RP and OP change downward and upward, respectively. The band bending forces the light-induced electrons in the OP's CB and the holes in the RP's VB to recombine at the point of contact. Due to the coulombic attraction between holes and electrons, the light-driven electrons in the OP's CB and the holes in the RP's VB are likely to recombine at the junction[53,61]. The schematic illustration of S-scheme is given in Fig. 3a-c.

3 Carbon materials

Carbon materials are substances that contain a significant amount of carbon. Carbon is a versatile element that can form a wide variety of compounds with diverse properties. Carbon materials can be found in various forms including organic and inorgan-

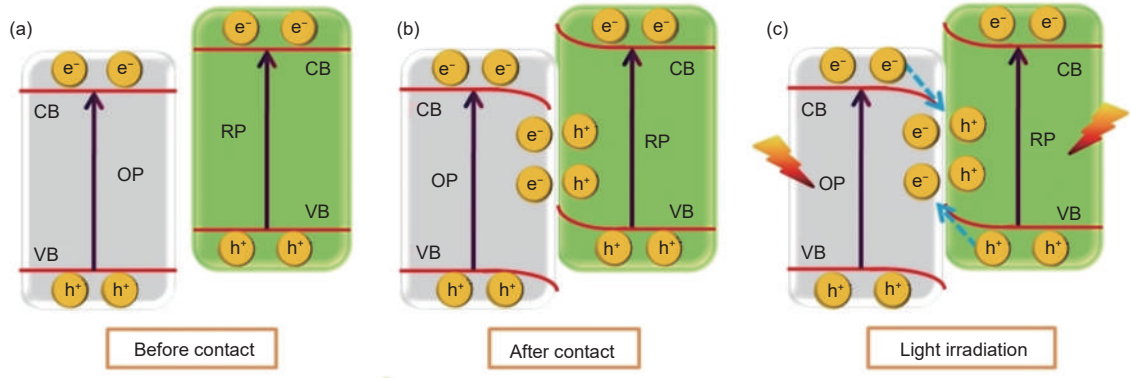

Fig. 3　Schematic illustration of S-scheme heterojunction (a) before contact, (b) after contact and (c) upon light irradiation

ic compounds. As also illustrated in Fig. 4, they involve a set of materials such as carbon nanotubes/nanofibers (CNTs/CNFs), fullerenes, carbon quantum dots (CQDs), graphene, graphene oxide (GO), reduced graphene oxide (rGO), graphdiyne (GDY), graphyne (GY), carbon sponge/aerogel etc[62,63]. Carbon's microstructure geometries and underlying intricate structures can vary across these various materials[64].

3.1　Role of carbon materials in photocatalysis

Carbonaceous nanomaterials have sparked a lot of interest in photocatalysis due to their fascinating features and capacity to be tuned by varying their structures and constituents[65]. These substances are an ideal alternative for this application due to their structural variance, electrical and thermal conductivity, huge surface area and extremely organized structure[66]. They are often utilized in water treatment processes due to their availability, affordability, excellent selectivity and non-toxicity[67]. Carbon materials' semiconducting properties may be advantageous in photocatalysis. They have a smaller fermi level compared to other semiconductors, making them suitable as co-catalysts. Semiconductor and carbonaceous compounds can link through the formation of solid chemical bonds, increasing photocatalytic ability by lowering the energy gap of semiconductor photocatalyst[68] while also decreasing the recombination rate of light-driven charges[69]. Their porous and highly structured arrangements allow for the inclusion of organic or inorganic functional groups, which can dramatically increase their photocatalytic efficiency. Quick electron transfer pathways and easier active site exposure are possible with porous architecture[70]. These materials offer a wide range of applications including the capacity to operate as a photosensitizer, semiconductor, support material, co-catalyst, and to decrease the band gap while accepting and transporting electrons[71]. Carbon materials' large surface area allows them to increase the total quantity of absorption sites for generating more H_2[72], which serves as the hub for adsorption and dissociation of water[68]. Furthermore, these materials can ensure the stability of coated nanoparticles by preventing cluster formation. Semiconductor nanoparticles may be implanted on the surfaces of carbon materials to improve their photocatalytic efficiency[73]. Their characteristics can be modified via incorporating functional groups, generating defects and integrating them with different semicon-

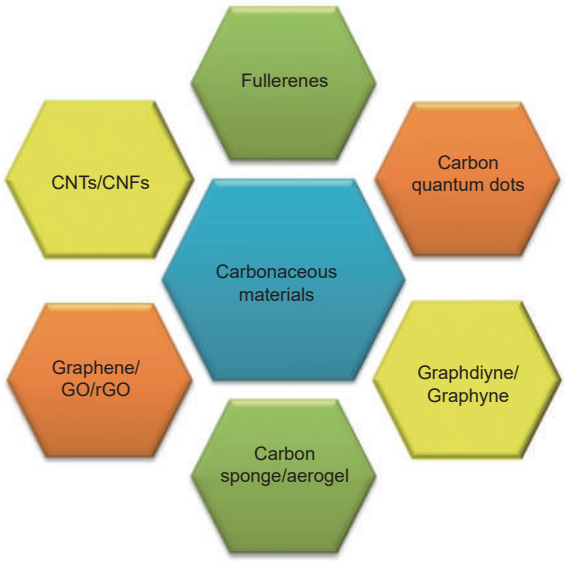

Fig. 4　Various types of carbon materials

ductor materials. They have better thermal conductivity and a greater work function compared to many semiconductors, allowing them to grab electrons from semiconductors' conduction bands, decreasing recombination rates[74].

3.2 Carbon nanotubes/nanofibers

With their vast surface area, fascinating electrical properties, distinct physicochemical features and elevated aspect ratio, CNTs and CNFs are promising contenders for designing and fabrication of novel photocatalysts[75,76]. CNTs may attach and swap sp^2 and sp^3 bonds for hybridization states under high pressure and have remarkable thermal and electrical properties, making them suitable for use in photocatalysis[77,78]. MWCNTs (multi-walled) have been shown to be far more effective in hydrogen generation than SWCNTs (single wall) or DWCNTs (double wall) because of their increased electrical conductivity, large aspect ratios and optical characteristics[79]. CNFs are 1-D nanomaterials having intriguing properties such as high electrical conductivity, low crystallinity, great mechanical strength, small surface area and low designing costs[80]. Hollow CNFs have many electrochemically active spots for redox reactions. Their porosity and regulated pore structure facilitate faster electron and ionic movement, resulting in improved rate capability and therefore popularity as a great catalyst support[81]. Wang et al. demonstrated the use of carbon solid nanofibers with Janus active sites as high performance catalysts for CO_2 reduction[82]. CNTs are used as electron mediators in photocatalytic systems for the development of g-C_3N_4/CNTs/CdZnS Z-scheme photocatalyst[83]. CNTs were observed in the gaps on the surface of photocatalyst through SEM image (Fig. 5a). HRTEM image in Fig. 5b revealed CdZnS nanoparticles of size 20 nm, and g-C_3N_4 and CNTs of diameter 20 nm. g-C_3N_4/CNTs/CdZnS showed highest H_2 evolution of 28.74 mmol g^{-1} h^{-1} (Fig. 5c). g-C_3N_4/CNTs/CdZnS has the lowest work function of 5.27 eV (Fig. 5d), which means the energy needed for light-induced electrons to escape is lowest and they can easily participate in photocatalytic reactions.

3.3 Carbon quantum dots (CQDs)

Carbon quantum dots have sparked significant excitement in photocatalysis because of their abundance, low toxicity, affordability and long lifespan[85]. The CQDs stand out from standard semiconductor quantum dots due to their improved water solubility, chemical and thermal stability[86], strong biocompatibility and convenience of production and functionalization[87]. They have a strong resistance to photo-bleaching which prevents photo-corrosion under light exposure, making them highly photostable and robust compared to metal-based alternatives[88,89]. 0-D carbon dots containing sp^2 carbon inserted by sp^3 carbon are effective electron transfer component for photo and Fenton-like catalysts[90,91]. CQDs can increase the photocatalytic performance of composite photocatalysts in a variety of ways. (1) CQDs operate as photosensitizers, increasing the absorption extent of UV and visible light. (2) CQDs operate as a donor/acceptor/accelerator for electron movement, preventing electron and hole recombination. (3) When CQDs are coupled with semiconductors, their expanded contact area boosts photocatalytic activity[92].

Xu et al. employed the carbon dots as co-catalyst for dual roles of solid-state electron mediator and electron acceptor for photocatalytic H_2 evolution using $ZnIn_2S_4$/carbon dots/g-C_3N_4[84]. The SEM image (Fig. 5e) revealed the stacked sheet-on-sheet structure of ZIS/CDs/CN, and HRTEM image (Fig. 5f) gave details about the heterojunction interfaces. The XRD and FTIR analysis before and after photocatalysis (Fig. 5g-h) demonstrated that the structural and functional groups of photocatalyst were intact. After contact, the directed propagation of electrons bends the energy band, generating an internal electric field (Fig. 5i).

3.4 Graphene/GO/rGO

Graphene has an sp^2 hybridized honeycomb-like framework with exceptional physical features such as increased hardness, high resistivity, strong elasticity and excellent flexibility, along with chemical qualities such as non-toxicity, good reactivity and so on[93]. Due to these features, graphene and its derivatives are typically used as flexible supports to promote light driven electron-hole separation[94]. GO has a signific-

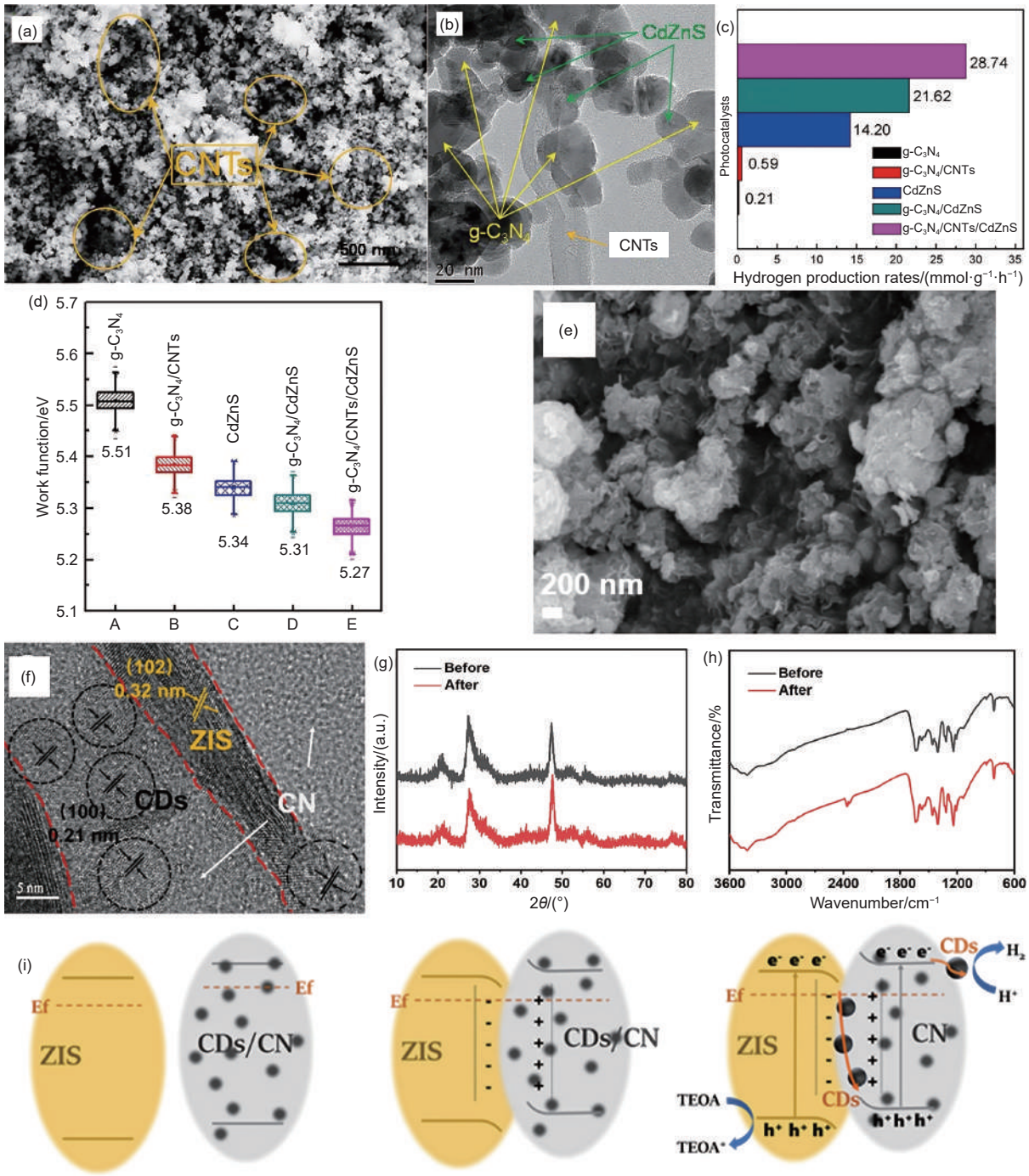

Fig. 5　(a) SEM and (b) HRTEM images of g-C_3N_4/CNTs/CdZnS. (c) Photocatalytic H_2 generation and (d) surface work function of prepared photocatalysts. Reproduced with permission from Elsevier[83]. (e) SEM and (f) HRTEM images of ZIS/CDs/CN composite. (g) XRD and FTIR spectra of ZIS/CDs/CN before and after photocatalysis. (i) S-scheme heterojunction mechanism between ZIS and CN before contact, after contact in dark and light. Reproduced with permission from Elsevier[84]

ant number of oxygen functional groups including carbonyl, epoxy, hydroxyl and carboxyl. Therefore, photocatalysts can bind strongly to these oxygen-rich functional groups and freely disperse on the GO surface, promoting its photocatalytic reduction[95]. GO has exceptional mechanical strength, high band gap, unique electrical properties, low density, wide surface area, ideal electron acceptor and transferring properties, all of which contribute to superior absorptivity, spatial distinction of charges and improved photocatalytic activity[96,97]. RGO exhibits more robust features than GO including enhanced optical properties, strong

electron mobility, chemical stability, large surface area[98], improved thermal conductivity, strong adsorption ability and outstanding flexibility[99]. Because of its high electrical mobility, it may efficiently divide light-induced electrons, exceeding the electron-hole recombination rate[100].

Gebreegziabher et al. reported a one-step chemical synthesis of GO and rGO straight from graphite powder in a solution of $KMnO_4$ and strong H_2SO_4 at different temperatures, facilitated by ultrasonication and without reduction step[101]. The STEM image of GO (Fig. 6a) revealed that it was thick, rough, disordered and had holes throughout its non-uniform sheet. The STEM picture of rGO revealed the existence of wrinkles and scrolls in its framework (Fig. 6b), indicating the existence of few-layered graphene sheets.

3.5 Graphdiyne/graphyne

Graphyne is novel carbon allotrope with 2D planar arrangement composed of sp- and sp^2-hybrid benzene rings bound by acetylene bonds. A common term graph-*n*-yne (where, n = 1, 2, 3…..) is referred to the total number of acetylenic chains between consecutive benzene rings[105]. The optimized geometrical configuration of GY was studied by Perveen et al (Fig. 6c)[102]. The structures of GYs govern their

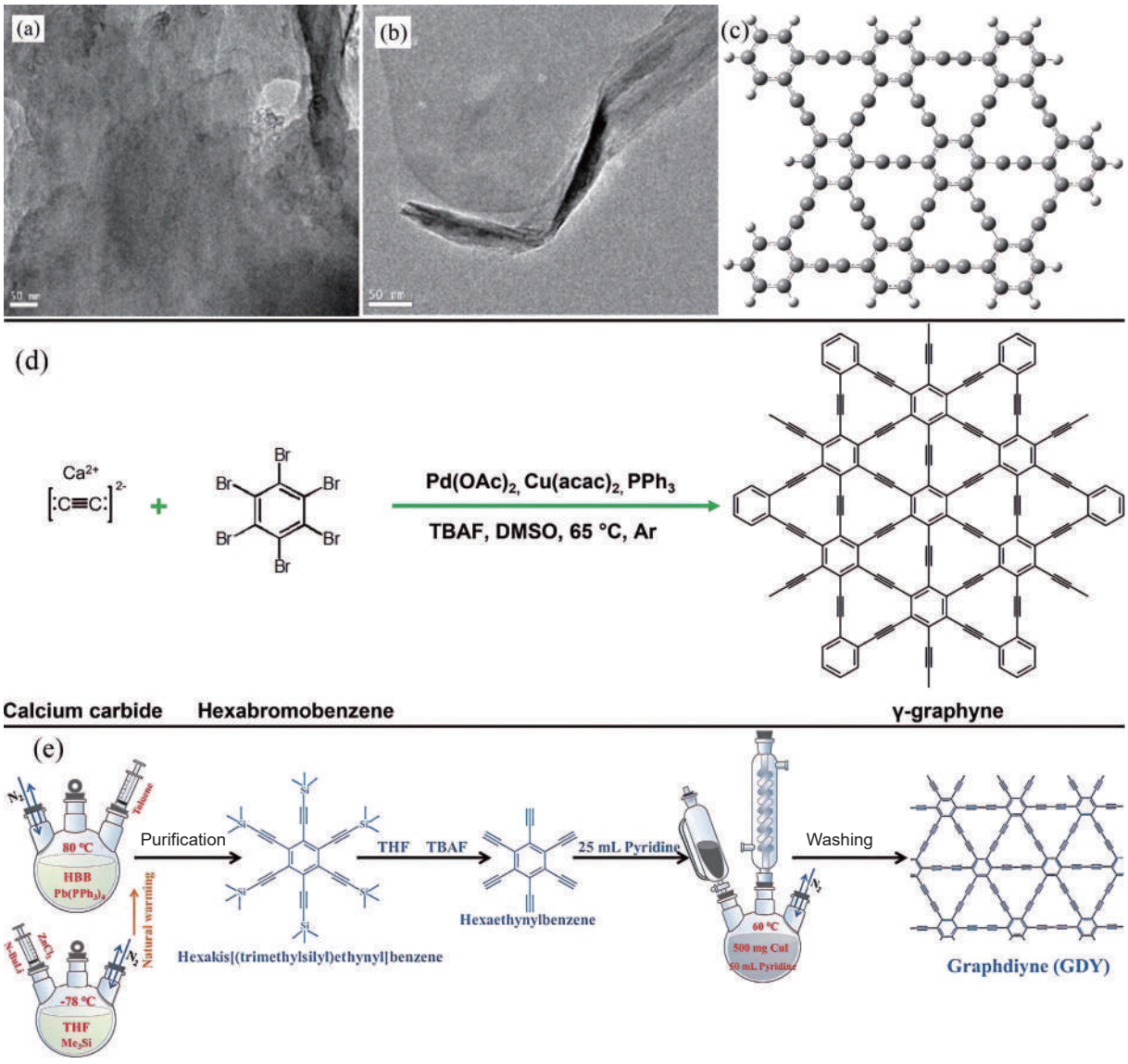

Fig. 6 STEM images of (a) GO and (b) rGO. Reproduced with permission from Elsevier[101]. (c) geometry of graphyne. Reproduced with permission from Elsevier[102]. (d) reaction for synthesis of γ-graphyne. Reproduced with permission from Elsevier[103]. (e) Synthetic route of GDY. Reproduced with permission from Elsevier[104]

physiochemical characteristics including non-uniform electronic structure, tunable band gaps[106], large carrier mobility[107], highly conjugated framework and evenly dispersed pores. The one-pot Sonogashira cross-linking technique reported by Barua et al (Fig. 6d)[103], generated large quantities of pure γ-graphyne under moderate circumstances. Graphynes are effective transporters and enhancers in photocatalytic processes due to their unique 2D properties and carbon-carbon bonding[105]. Graphdiyne (GDY) has diacetylene linkage, triangular hole structure, simple synthesis and adjustable band gap[108]. The C≡C give GDY a number of intriguing properties such as excellent electronic conductivity, high stability and favoured catalytic function[109]. GDY has a customizable band gap, porous structure and large surface area. The experimental synthesis of diverse GDYs is in high demand[40]. Fan et al. constructed a simple synthetic route for GDY (Fig. 6e)[104].

3.6 Fullerenes

Fullerenes are surrounded by cage-like constructions of twelve pentagon rings and a larger number in the form of 6-member rings joined by carbon atom positions. Buckyball (C_{60}) has 32 sides, 12 pentagons and 20 hexagons, and the entirety of carbon atoms are connected in a truncated icosahedron with 60 vertices[11,110]. In spherical C_{60}, the angle between two σ bonds is 106° and the angle between σ and π bonds is 101.64°. The molecule's radius is around 0.335 nm. C_{60} molecules in solids are thermodynamically chaotic and anisotropic[111,112]. Fullerenes are electronegative molecules that allow for quick light-induced electron transport since the majority of their π orbitals are located outside the cage. The electronic framework of C_{60} is naturally centred on the surface of 30 π-orbitals[113]. C_{60} has numerous physical and chemical features including solubility, superconductivity, non-hazardous, limiting effects and so on. Its unique features in photocatalysis constitutes distinct morphological features, optical physical qualities when activated by light and derivatives generated by other functional groups[112].

There have been a few studies where C_{60} is used to create hybrid photocatalysts having superior photocatalytic efficiency[114,115]. A Z-scheme photocatalyst C_{60}/TpPa was produced by He et al. for CO_2 reduction using in-situ solvothermal technique[116]. TpPa-1, which has porous structure, efficient light absorption and large number of reaction sites, can be used to create a variety of structures. The study found that C_{60}/TpPa has maximal CO production rates of 48.16 μmol g^{-1} h^{-1} and 90.25 μmol g^{-1} h^{-1} in pure CO_2 and 10% CO_2 environments, respectively.

3.7 Carbon sponge/aerogel

This novel concept involves securing three-dimensional (3D) open-cell components such as aerogels and sponges onto carbonaceous substrates with 3D open-cell structures. The following are the advantages of such systems: (1) Highly porous and strong pore connectivity can guarantee quick reactant movement. (2) Open-cell 3D structures can offer a more viable surface for photocatalyst loading. (3) 3D monolithic photocatalysts can be easily gathered and isolated from the reaction system[117]. Carbon aerogels often have 3D interlinked structures joined by main nanoparticles. Their microporous structural characteristics are linked to the intra-particle arrangement, while interparticle morphology controls the formation of mesopores and macropores[118]. Carbon aerogel micropore and mesopore development may be regulated separately, which is a significant advantage for fabricating porous materials[119]. Carbon aerogels possess unique physical characteristics such as low density, vast surface area, porous structure, excellent electrical conductivity, chemical stability and ecological suitability[120]. Their enormous specific surface areas and macroscopic morphologies allow for homogeneous immobilization of active compounds on substrates[121].

3.8 Synthesis routes of carbon based Z-scheme and S-scheme heterojunctions

The carbon materials can be incorporated with other semiconductors to form Z-scheme and S-scheme heterojunctions through various routes such as hydrothermal or solvothermal[122,123], calcination[124], sonication[125], co-precipitation[126], self-assembly etc[127]. The specific synthesis route depends on the type of car-

bonaceous material, other semiconductor, desired properties of heterojunctions and control over synthesis conditions[128]. Influenced by the varied benefits, tremendous attention has been directed towards the fabrication of carbon materials based Z-scheme and S-scheme heterojunctions to achieve good photocatalytic outputs. The hydrothermal or solvothermal process refers to the chemical reaction of substances in a sealed solution comprising water or organic solvent, respectively, cooked beyond room temperature and pressure. Because of its environmental friendliness and low cost, this approach is commonly used to make carbonaceous-based heterojunctions[129]. Liu et al. reported a simple hydrothermal approach to synthesize the direct Z-scheme $Cd_xZn_{1-x}S$-Fe_2O_3/rGO nanocomposite as multi-functional photocatalyst (Fig. 7a)[122]. The Fe_2O_3 quantum dots (QDs) are bound to $Cd_xZn_{1-x}S$ when —COO groups and $Cd_xZn_{1-x}S$-Fe_2O_3 QDs heterojunctions occur rapidly on the surface of rGO due to van der Waals forces. The energy gap of $Cd_xZn_{1-x}S$ is changed by varying the molar ratio of Zn^{2+} to Cd^{2+} ions. The high-efficiency transit and division of light-induced electron-hole pairs, as well as the presence of more catalytic active sites and an enormous specific surface area, all contribute to exceptional photocatalytic performance.

The self-assembly technique is affordable, easy to use and does not necessitate harsh conditions or supplementary chemical reagents, making it a green synthetic process that is commensurate with the ecological benefits of carbonaceous photocatalysts[132]. Liu et al. combined RGO with HCl protonation of g-C_3N_4 (H—CN) using an electrostatic self-assembly approach to create distinct *X*% RGO/H—CN 2-D nanocomposites as demonstrated (Fig. 7b)[130]. RGO, as a conductive substrate, immobilizes H—CN, resulting in powerful interfacial contact that improves carrier division and promotes greater light-driven electron abundance on the surface. RGO-5 (GO processed at 120 °C for 5 h) had the greatest defect density and C—OH/C—O—C content, resulting in the best photocatalytic and thermal-assisted photocatalytic efficiencies.

Sonication procedure involves exposing metallic

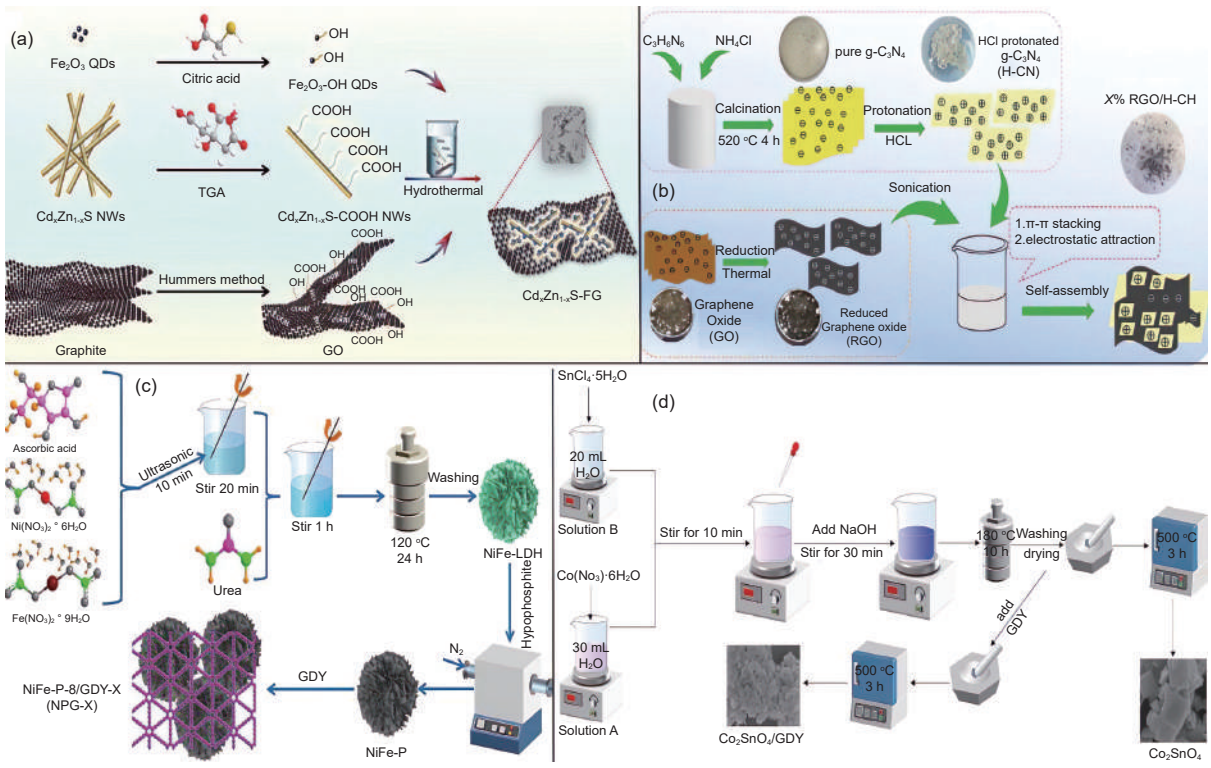

Fig. 7 (a) Hydrothermal synthetic route of $Cd_xZn_{1-x}S$-FG. Reproduced with permission from Elsevier[122]. (b) Self-assembly synthesis of *X*% RGO/H-CN. Reproduced with permission from Elsevier[130]. (c) Ultrasonication synthetic route of NiFe-LFD, NiFe-P and NPG-*X*. Reproduced with permission from Elsevier[104]. (d) Calcination synthesis of CO_2SnO_4 and Co_2SnO_4/GDY-*x*. Reproduced with permission from Elsevier[131]

salt solutions to vigorous ultrasonic vibrations which disintegrate the materials' chemical bonds. These vibrations generate acoustic cavitation which is the development, growth and implosive burst of bubbles in solution, resulting in extraordinarily elevated pressures and temperatures[133]. A low cost S-scheme NiFe-P/GDY photocatalyst was developed by Fan et al. through ultrasonication and stirring method by phosphorylation of NiFe-P and then its combination with GDY as illustrated in (Fig. 7c)[104]. The flowery layered double hydroxide of NiFe serves as an anchoring skeleton for Ni_2P and GDY. The outstanding conductivity of GDY and S-scheme heterojunction could efficiently transport light-induced electrons from CB of NiFe-P to VB of GDY, inhibiting electron-hole recombination and attaining spatial division of carriers, thus enabling the progression of catalytic reactions.

Calcination is a thermal treatment or annealing procedure used to decompose solid minerals or ores in the absence of oxygen or air. This strategy has various advantages including a straightforward production method and high crystallinity of the resulting nanoparticles[134,135]. A Co_2SnO_4/graphdiyne photocatalyst was formed by Guo et al. through the calcination of graphdiyne and $CoSn(OH)_6$ together after grinding and mixing them (Fig. 7d). The high-temperature calcination architecture strongly coupled Co_2SnO_4 alongside graphdiyne, resulting in larger contact area, greater number of active sites and quicker light-induced electron transport[131]. The catalyst synthesis process used in this study is novel, providing a generic and high-efficiency approach for utilizing the graphdiyne-based S-scheme heterojunction to solar energy conversion application.

4　Applications of carbon materials based Z-scheme and S-scheme heterojunctions

With their excellent electron-hole separation ability and substantial solar energy utilization, carbon materials based photocatalysts provide exceptional performance for applications such as H_2 production and CO_2 reduction. Thus, some earlier reported such works of carbonaceous based Z-scheme and S-scheme heterojunctions with remarkable photocatalytic performance are summarized in this part.

4.1　Photocatalytic H_2 generation

In a frantic attempt to avert another energy crisis, hydrogen (H_2), which emits no pollutants, is not dependent on non-renewable fossil fuels. Water splitting used in photocatalytic H_2 generation is an effective way to address the energy dilemma[136]. Solar water splitting is gaining a lot of attention since it can transform solar radiation into chemical energy that can be stored as carbon-free H_2 fuel. As a result of the redox reaction caused by light exposure on the photocatalytic surface, water is divided into hydrogen and oxygen[137].

A well-organized Z-scheme $ZnIn_2S_4$-S/CNTs/RP (ZIS-S/CNTs/RP) photocatalyst was created by Lui et al. using an energy band alignment steering technique to achieve excellent photocatalytic H_2 production[25]. ZIS-S/CNTs/RP has much better photocatalytic H_2 generation of 1 639.9 μmol g^{-1} h^{-1}, compared to pure red phosphorus (RP), CNTs/RP and ZIS-S/RP composites (Fig. 8b-c). The PL and EIS spectra of ZIS-S/CNTs/RP, ZIS-S/CNTs/BRP and ZIS/CNTs/RP (Fig. 8d-e), demonstrated lower electron-hole recombination rate of ZIS-S/CNTs/RP and charge transfer resistance which may be attributed to interfacial charge segregation and movement in the heterojunction. The ESR signal (Fig. 8a), gave direct information about the sulphur vacancies as ZIS-S exhibited strong signal at 324 mT. The alteration of nano-sized RP and the emergence of sulfur vacancies in $ZnIn_2S_4$ resulted in a customized energy band alignment of the heterojunction featuring greater reduction potential and bigger Fermi level potential difference. The Z-scheme reaction mechanism of ZIS-S/CNTs/RP heterojunction is shown in Fig. 8f.

Jin et al. also developed an S-scheme heterojunction between the contact interfaces of WO_3 nanorods comprising surface defects and GDY-Cu sample for H_2 generation activity[138]. GDY-Cu/WO_3 sample exhibits the highest H_2 production of 2 072 μmol g^{-1} h^{-1},

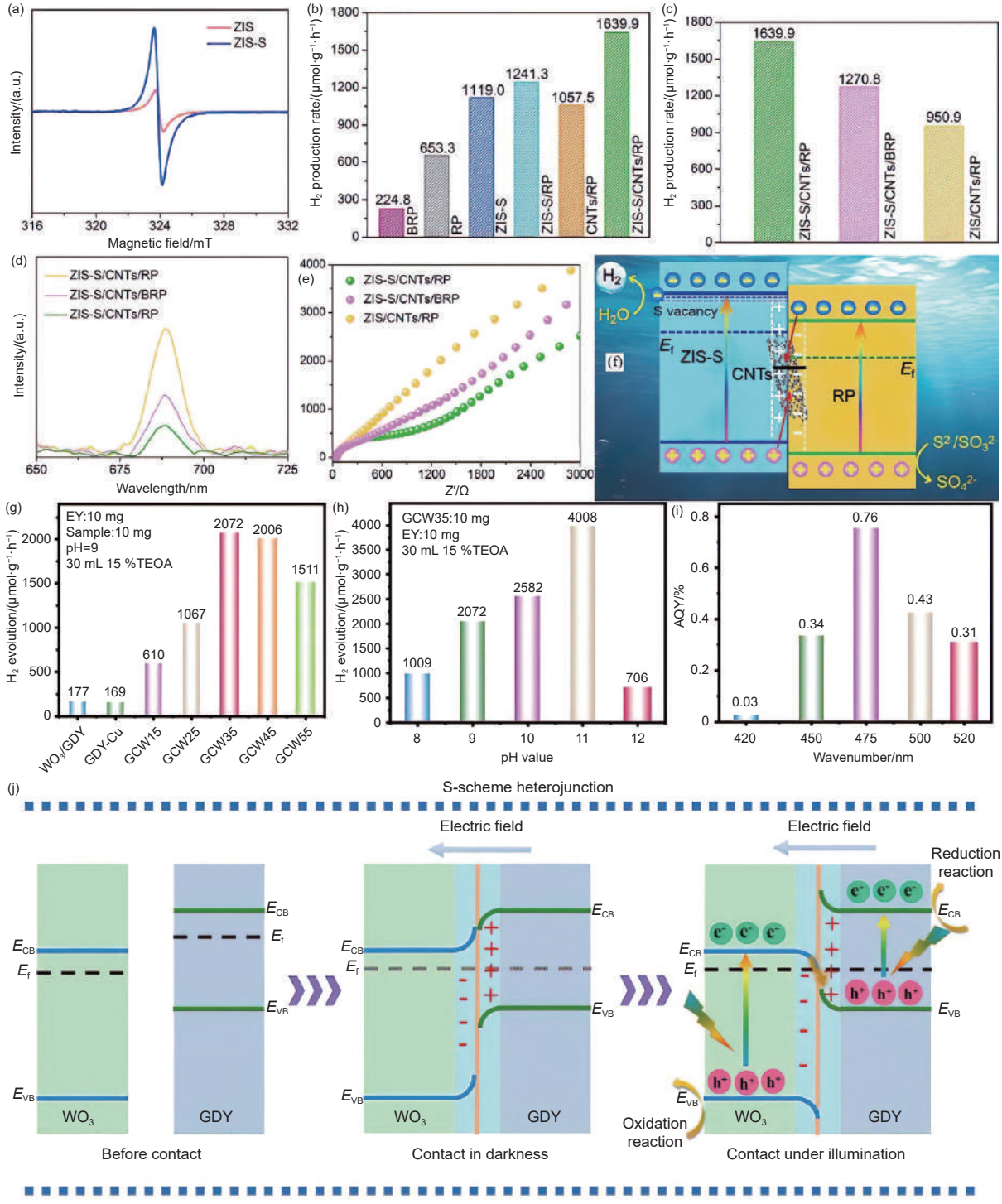

Fig. 8 (a) ESR spectra of ZIS-S and ZIS. (b) H_2 generation rate over various photocatalysts. (c) H_2 generation performance of ZIS-S/CNTs/RP, ZIS-S/CNTs/BRP and ZIS/CNTs/RP. (d-e) PL spectra and EIS Nyquist plots of ZIS-S/CNTs/RP, ZIS-S/CNTs/BRP and ZIS/CNTs/RP. (f) Proposed photocatalytic H_2 generation mechanism over Z-scheme ZIS-S/CNTs/RP heterojunction. Reproduced with permission from Elsevier[25]. (g) H_2 evolution performance of various photocatalysts. (h) H_2 evolution performance of GCW35 at different pH. (i) AQE of GCW35 at different wavelengths. (j) charge transfer paths of WO_3/GDY S-scheme heterojunction. Reproduced with permission from Elsevier[138]

reaching 12.2 times that of GDY-Cu (Fig. 8g). The catalyst has even greater H_2 production capability in TEOA solution over pH 11, reaching 4 008 μmol g^{-1} h^{-1} (Fig. 8h). The AQE value of GCW35 reached 0.76% at 475 nm in Fig. 8i. The addition of GDY-Cu ohmic junction creates more active sites and thereby more electrons for photocatalytic processes. The H_2 generation activity of GCW35 composite has been signific-

antly increased by the synergistic impact of S-scheme heterojunction and ohmic junctions. Fig. 8j depicts the electron movement of the GDY/WO_3 S-scheme heterojunction in photocatalytic processes. The recent advances in carbon based Z-scheme and S-scheme heterojunctions for photocatalytic H_2 generation are summarized in Table 1.

4.2 Photocatalytic CO_2 reduction

Given that global warming poses a major hazard to life, excessive CO_2 emissions are a major contributing factor to it. Various methods have been devised to reduce the atmospheric concentration of CO_2 such as absorption, bioconversion and photocatalytic reduction[164]. It is advantageous to use photocatalysis to transform atmospheric CO_2 into different hydrocarbon fuels for lowering its concentration. The generated species reveal a connection between the targeted CO_2 product's reduction potential and semiconductors' CB edge potential. The fundamental steps in such reactions are the adsorption of carbon dioxide on the active sites of photocatalysts and the transformation of photon energy through photocatalysis to form charge carriers[137]. Deng et al. created a CDs-modulated S-scheme heterojunction of CDs/NiAl-LDH@In_2O_3 (C-DH@IN) using a simple in-situ hydrothermal technique for selective photo-reduction of CO_2 into CH_4[165]. C-DH@IN's multi-shell nanotube framework results in greater CH_4 formation rate of 10.67 μmol h^{-1} g^{-1} and greater CH_4 selectivity (85.70%) in comparison to In_2O_3 and NiAl-LDH@In_2O_3 binary catalysts (Fig. 9a-b). The EIS Nyquist plots in Fig. 9c displayed smallest arc radius of 3%C-DH@IN revealing its low resistance and good charge transfer capabilities. The DMPO− $\cdot O_2^-$ and DMPO− ·OH signals were clearly observed in ESR spectra in Fig. 9d which verified the strong redox ability of C-DH@IN. The proposed S-scheme heterojunction for photocatalytic CO_2 reduction reaction over C-DH@IN is shown in Fig. 9e.

Li et al. also constructed an S-scheme 2D-1D-2D sandwich photocatalyst for CO_2 photo-reduction where g-C_3N_4 nanosheets were primary photocatalyst and rod-like CeO_2 (R-CeO_2) with exceptional $Ce^{4+}\rightarrow Ce^{3+}$ conversion property and rGO were loaded on the g-C_3N_4 surface[166]. Using rGO/R-CeO_2/g-C_3N_4 as a catalyst resulted in CO and CH_4 production of 63.18 and 32.67 μmol g^{-1} after 4 h, which were approximately 4 and 6 times greater than bare CN, respectively (Fig. 9f). Cyclic testing demonstrated that the composite was highly photocatalytic and material stable (Fig. 9g). The smaller arc radius of 3RCCN in the EIS spectra (Fig. 9h), demonstrated its greater electron transfer ability. The band gap structure and CO_2 photo-reduction mechanism of 3RCCN multi-interface contact heterojunction is shown in Fig. 9i. The recent advances in carbon based Z-scheme and S-scheme heterojunctions for photocatalytic CO_2 reduction are summarized in Table 2.

5 Bottlenecks, economic viability and environmental implications

The environmental impact of utilizing carbonaceous photocatalysts may be both positive and negative, depending on the application and the possibility of unexpected repercussions. Various carbonaceous photocatalysts have shown enhanced photocatalytic performances, making them promising for environmental remediation and sustainable energy production with safety and low synthesis costs[186]. The carbon nanotubes have less purity, develop defects during functionalization and expensive fabrication techniques. In addition, the multi-walled CNTs do not display good electrical property as single-walled CNTs. Also, their agglomeration leads to poor dispersibility[71]. The production and disposal of carbonaceous photocatalysts can have a carbon footprint, which may contribute to greenhouse gas emissions. However, the use of renewable energy sources for the synthesis of these materials can help mitigate this impact. Some carbon-based nanomaterials, such as graphene and carbon quantum dots, may have toxic effects on living organisms. This is a concern that needs to be addressed through careful material selection and proper disposal methods. In some cases, the degradation of organic pollutants by photocatalysts may not completely eliminate them but rather convert

Table 1 Recent advances in carbon based Z-scheme and S-scheme heterojunctions for photocatalytic H_2 generation

Photocatalyst (dosage)	Synthesis method	Sacrificial agent	Light source/ Intensity	AQE	Performance	Refs.
$ZnIn_2S_4$-S/CNTs/RP (30 mg)	Directed assembly	Na_2S & Na_2SO_3	Xe lamp, 300 W	–	1639.9 μmol/g/h	[25]
g-C_3N_4/CNTs/CdZnS (50 mg)	Hydrothermal	Na_2S & Na_2SO_3	Xe lamp, 300 W	–	28.74 mmol/g/h	[83]
$Zn_3V_2O_8$/MWCNT (50 mg)	Hydrothermal	Glycerol	Xe lamp	–	99.55 μmol/g/h	[139]
$ZnIn_2S_4$/carbon dots/g-C_3N_4 (25 mg)	Calcination and water bath	TEOA	Xe lamp, 300 W	12.73% at 420 nm	17.58 mmol/g/h	[84]
g-C_3N_4/NCDS/MoS_2 (0.05 g)	Thermal polymerization and solvothermal	TEOA	Xe lamp, 300 W	–	212.41 μmol/g/h	[140]
C dots decorated g-C_3N_4/TiO_2 (50 mg)	Solvothermal and calcination	TEOA	LED lamps, 12 W	–	580 μmol/g/h	[141]
g-C_3N_4/NCDs (50 mg)	Calcination	TEOA	Xe lamp, 300 W	29.8% at 420 nm	3319.3 μmol/g/h	[142]
g-C_3N_4/NCDs/WO_x (20 mg)	In-situ growth	TEOA	Xe lamp, 300 W	7.58% at 420 nm	3.27 mmol/g/h	[143]
C_3N_4 nanotube/NCDs/Ni_2P (50 mg)	Hydrothermal and calcination	TEOA	Xe lamp, 300 W	–	627.2 μmol/g/h	[144]
SnO_2/NPCDs/CNNT (10 mg)	Sonication	TEOA	Monochromatic light	18.91% at 420 nm	10.73 mmol/g/h	[145]
N-CDs/S-C_3N_4 (50 mg)	π-π conjugate self-assembly	TEOA	Xe lamp	4.67% at 420 nm	483.76 μmol/g/h	[146]
$Cd_xZn_{1-x}S$-Fe_2O_3/rGO (50 mg)	Hydrothermal	Na_2S & Na_2SO_3	Xe lamp, 300 W	–	26.8 mmol/g/h	[122]
$Cd_{0.5}Zn_{0.5}S$/RGO/g-C_3N_4 (30 mg)	Solvothermal	Na_2S & Na_2SO_3	Xe lamp, 300 W	37.88% at 420 nm	39.24 mmol/g/h	[147]
$LaFeO_3$/g-C_3N_4-graphene (50 mg)	Calcination	TEOA	Xe lamp, 300 W	–	1326.5 μmol/g/h	[124]
$AgIO_4$/ZnO/graphene	Ultrasonication	Methanol	Xe lamp, 300 W	–	16.4 mmol/g/h	[148]
TiO_2/RGO/$LaFeO_3$ (10 mg)	Hydrothermal	Methanol	Xe lamp, 300 W	7.1% at 380 nm	0.893 mmol/g/h	[149]
$ZnIn_2S_4$/rGO/CeO_2 (15 mg)	Hydrothermal	Na_2S & Na_2SO_3	Xe lamp, 150 W	–	2855 μmol/g/h	[150]
WO_3/TiO_2/rGO (50 mg)	Hydrothermal	Methanol	Xe lamp, 350 W	–	245.8 μmol/g/h	[58]
rGO supported TiO_2/$In_{0.5}WO_3$ (0.1 mg/mL)	Wet impregnation	Glycerol	Xe lamp	15.6% at 365 nm	309.98±11.4 μmol/g/h	[151]
Rh-ZnO/rGO/ZnS (30 mg)	In-situ micro-cell growth & kinetic ion-exchange	Na_2S & Na_2SO_3	Xe lamp, 300 W	11.02% at 365 nm	2686 μmol/g/h	[152]
$Mn_{0.2}Cd_{0.8}S$/$CoFe_2O_4$/rGO (50 mg)	Electrostatic interaction	Na_2S & Na_2SO_3	Xe lamp, 300 W	–	133.5 μmol/g/h	[153]
$LaFeO_3$/RGO (0.5 g/L)	Hydrothermal	Methanol	Xe lamp, 250 W	–	82 mmol/g/h	[154]
TiO_2/rGO/g-C_3N_4 (5 mg)	Pulsed laser ablation in liquids	Glycerol	Xe lamp, 300 W	10.95% at 450 nm	32±1 mmol/g/h	[155]
n-ZnS/rGO/p-Bi_2S_3 (0.01 g)	Hydrothermal	Na_2S & Na_2SO_3	Xe lamp, 100 W	–	2523.4 μmol/g/h	[156]
CdS-rGO-WO_3 (13 mg)	Hydrothermal	Methanol	Solar simulator, 100 W	2.49% at 420 nm	11.69 mmol/g/h	[157]
γ-GY/$CuMoO_4$ (10 mg)	Hot solvent	TEOA	Xe lamp, 300 W	–	197 μmol in 5 h	[158]
Co_2SnO_4/graphdiyne (10 mg)	Calcination	TEOA	LED light, 5 W	–	8.79 mmol/g/h	[131]
GDY/MoP (10 mg)	Physical mixing	TEOA	Xe lamp, 300 W	–	8876.4 μmol/g/h	[159]
GDY-Cu/WO_3 (10 mg)	Stirring and evaporating solvent	TEOA	LED light, 5 W	0.76% at 475 nm	4008 μmol/g/h	[138]
CoS_2/GDY (10 mg)	Low-temperature water bath	TEOA	LED, 5 W	1.52% at 475 nm	1835 μmol/g/h	[160]
CuI-GDY/ZnAl LDH (10 mg)	Self-assembly	TEOA	Xe lamp, 300 W	0.15% at 420 nm	28.60 μmol in 5 h	[161]
GDY/g-C_3N_4-V_N (6 mg)	Sonication	TEOA	LED lamp, 5 W	–	17.87 μmol/h	[125]
GDY/$CoTiO_3$ (10 mg)	In-situ calcination	TEOA	LED, 5 W	5.45% at 420 nm	716 μmol/g/h	[162]
NiFe LDH/GDY (20 mg)	Ultrasonic and stirring	–	Xe lamp, 300 W	–	928 μmol/g/h	[104]
CdS-g-C_3N_4-GA (50 mg)	Ultrasound	TEOA	Xe lamp, 300 W	–	86.38 μmol/g/h	[29]
g-C_3N_4/TiO_2/$ZnIn_2S_4$ graphene aerogel (100 mg)	Isoelectric point assisted calcination	Methanol	Xe lamp, 300 W	–	6531.9 μmol/g	[163]

them into other forms that may still pose environmental risks[187]. While carbon materials offer promising environmental benefits, it is essential to consider their potential impacts and work towards minimizing the negative effects.

In terms of economic viability, research on photocatalytic CO_2 reduction is expanding, with an emphasis on tackling global environmental issues and meeting future energy demands[188]. While there are still limitations, the introduction of carbonaceous photocatalysts has opened up possibilities for investigating ecologically friendly and energy-efficient synthesis processes. The use of carbon materials in photocatalysis holds promise for the development and production of efficient and cost-effective photocatalysts[189].

6 Conclusion, challenges and outlook

In conclusion, it has been demonstrated that car-

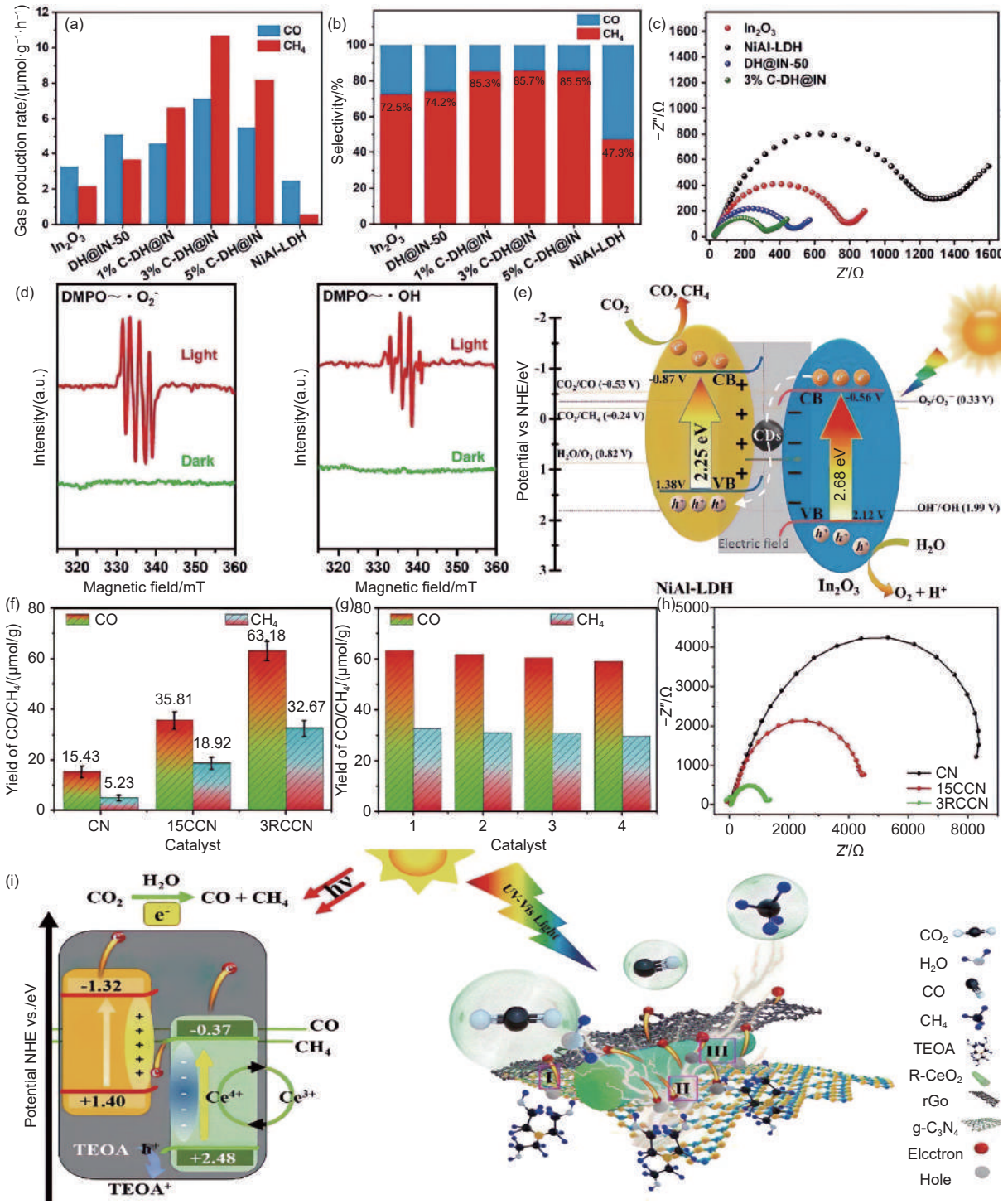

Fig. 9　(a) Photoreduction performance of various photocatalysts, (b) carbon products selectivity of catalysts, (c) EIS Nyquist plots of In_2O_3, NiAl-LDH, DH@IN-50 and 3%C-DH@IN, (d) DMPO- $\bullet O_2^-$ and DMPO- •OH spin-trapping ESR spectra of 3%C-DH@IN, (e) charge transfer mechanism over C-DH@IN, Reproduced with permission from Elsevier[165]; (f) CO and CH_4 yields for various photocatalysts, (g) cycling experiments, (h) EIS curves of CN, 15CCN and 3RCCN, (i) band gap structure and CO_2 photo-reduction mechanism of 3RCCN multi-interface contact composite, Reproduced with permission from Elsevier[166]

bon materials are crucial for the preparation and design of sophisticated photocatalysts and a large number of carbonaceous based photocatalysts have been created. The remarkable progress made by carbonaceous photocatalysts provides a means of investigating the use of carbon in photocatalysis. The excellent qualities of different carbon materials and their variable characteristics present many opportunities for

Table 2 Recent advances in carbon based Z-scheme and S-scheme heterojunctions for photocatalytic CO_2 reduction

Photocatalyst (Dosage)	Synthesis method	Light source/ Intensity	Performance	Refs.
g-C_3N_4/CDs/WO_3 (20 mg)	Confined co-assembly	Xe lamp, 300 W	CO = 31.04 μmol/g/h	[167]
CPDs/$Bi_4O_5Br_2$ (30 mg)	Co-precipitation	Xe lamp, 300 W	CO = 132.42 μmol/g/h	[126]
CQDs/$Bi_{12}O_{17}Cl_2$/NiAl-LDH (50 mg)	One-pot hydrothermal	Xe lamp, 300 W	CO = 16.4 μmol/g/h	[168]
CDs/NiAl-LDH@In_2O_3 (5 mg)	In-situ hydrothermal	Xe lamp, 300 W	CH_4 = 10.67 μmol/g/h CO = 7.12 μmol/g/h	[165]
CPDs/$Bi_{12}O_{17}Cl_2$ (30 mg)	Mechanical stirring	Xe lamp, 300 W	CO = 3.21 μmol/g/h	[169]
Ag_2CrO_4/g-C_3N_4/GO (100 mg)	Self-assembly	Xe lamp, 300 W	CH_3OH+CH_4 = 1.03 μmol/g in 3 h	[170]
O-ZnO/rGO/UiO-66-NH_2 (0.1 g)	Solvothermal	Xe lamp, 300 W	CH_3OH = 34.83 μmol/g/h HCOOH = 6.41 μmol/g/h	[123]
α-Fe_2O_3/graphene/Bi_2O_2S (50 mg)	Impregnation-hydrothermal	Xe lamp, 300 W	CO = 13 μmol/g/h CH_4 = 4.27 μmol/g/h C_2H_4 = 2.88 μmol/g/h	[171]
g-C_3N_4/ZnO/GA (10 mg)	Self-assembly with co-precipitation	Xe lamp, 300 W	CO = 33.87 μmol/g/h	[172]
RGO/H-CN (5 mg)	Self-assembly	Xe lamp, 300 W	CO = 10.21 μmol/g CH_4 = 5.56 μmol/g	[130]
g-C_3N_4/BiOI/RGO on Ni foam	Reduction	Xe lamp, 300 W	CO = 21.85 μmol/g in 8 h	[173]
α-Fe_2O_3/amine-RGO/$CsPbBr_3$	Solvent evaporation-deposition	Xe lamp, 150 W	CH_4+CO+H_2 = 469.16 μmol/g in 40 h	[174]
MoS_2/SnS_2/rGO (20 mg)	Solvothermal	Mercury lamp, 8 W	CO = 68.53 μmol/g/h CH_4 = 50.55 μmol/g/h	[175]
ZnV_2O_6/rGO/g-C_3N_4 (100 mg)	One-pot solvothermal	Hg lamp, 200 W	CO = 2802.9 μmol/g/h	[176]
$CsPbBr_3$/USGO/α-Fe_2O_3 (4 mg)	Ultrasonication	Xe lamp, 300 W	CO = 73.8 μmol/g/h	[177]
ZnV_2O_6/RGO/g-C_3N_4 (100 mg)	Solvothermal	Xe lamp, 35 W	CH_3OH = 3438 μmol/g	[178]
rGO/$InVO_4$/Fe_2O_3 (100 mg)	Deposition-precipitation	LED light, 20 W	CH_3OH = 16.9 mmol/g	[179]
g-C_3N_4-RGO-NH_2-MIL-125(Ti) (100 mg)	Hydrothermal	HID Xe lamp, 35 W	CO = 383.79 μmol/g CH_4 = 13.8 μmol/g	[180]
Bi_2WO_6/RGO/g-C_3N_4 (50 mg)	Hydrothermal	Xe lamp, 300 W	CO = 15.96 μmol/g/h	[181]
CoAl-LDH/RGO/$InVO_4$ (50 mg)	Hydrothermal	Xe lamp, 300 W	CO = 204.86 μmol/g/h	[182]
g-C_3N_4/rGO/ZnV_2O_6 (0.1 g)	One-pot solvothermal	HID Xe lamp, 35 W	CH_3OH = 6246.1 μmol/g	[127]
g-C_3N_4/R-CeO_2/rGO (100 mg)	Hydrothermal	Xe lamp, 300 W	CO = 63.18 μmol/g in 4 h CH_4 = 32.67 μmol/g in 4 h	[166]
CoZnAl-LDH/RGO/g-C_3N_4 (50 mg)	Hydrothermal	Xe lamp, 300 W	CO = 10.11 μmol/g/h	[183]
g-C_3N_4/Ag_3VO_4/rGO (0.05 g)	Hydrothermal	UV-vis light	CO = 7.03 μmol/g/h	[184]
MXene/GO/PDI (10 mg)	Impregnation	Xe lamp, 350 W	CH_3OH = 771.1 μmol/g/h	[185]
C_{60}/TpPa	In-situ solvothermal	LED lamp, 40 W	CO = 90.25 μmol/g/h	[116]

the fabrication of new carbonaceous photocatalysts with fascinating specific functions as well as excellent practical accomplishment in both scientific and commercial communities. Carbonaceous photocatalyst development has advanced significantly, but there are still a number of significant obstacles that must be removed to encourage their widespread use. The following points can be used to summarize our quick overview of the current challenges with different carbon materials and our reasonable perspectives for the future for the advancement of carbonaceous photocatalysts.

Most of the time, semiconductors are deposited onto the surface of carbon matrix. Consequently, the interface connection between the semiconductor and carbon phase is not very intimate which limits the bonding force and electron transfer capacity. Thus, by maximizing the compatibility of carbon phase and semiconductors, the fundamental characteristics of carbon materials based photocatalysts such as energy gap, charge separation effectiveness and light absorption ability of photocatalysts might be enhanced further.

Despite being a plentiful element on Earth, carbon materials only serve as co-catalysts and substrates in composite systems because of their low photocatalytic ability and the majority of commanding role semiconductors are insufficient. As a result, it is crucial to identify the carbon-based process that improves photocatalytic performance—a mechanism that is currently unclear. A better knowledge of enhancing mechanism would enable more effective use of semi-

conductors which would lower the price of composite photocatalysts—a cost that is essential for real-world applications.

Many studies have been conducted to challenge the current manufacturing procedures for carbonaceous nanomaterials which are deemed to be highly challenging and unproductive[11]. The production of carbonaceous photocatalytic compounds should study energy-efficient and ecologically friendly methods while also taking into the materials' applications and potential commercial advantages.

The photocatalytic efficiency of composite materials is effectively increased by nanostructured carbons which include carbon dots, graphene and CNT. However, because of their powdered macroscale anatomy, these catalysts are hard to recover after the reaction and can accidentally leak, causing secondary pollution. Consequently, 3D carbon-based photocatalysts have been produced and 3D monolithic photocatalysts are the chosen type.

Declaration of interests

The authors declare that they have no known competing financial interests or personal relationships that could have appeared to influence the work reported in this paper.

The authors declare no conflict of interest.

Acknowledgements

This research was funded by the following grants, including the Key Research and Development Program of Shaanxi Province (No. 2023-LL-QY-42), the Xi'an University of Architecture and Technology Research Initiation Grant Program (No. 1960323102), and the Xi'an University of Architecture and Technology Special Program for Cultivation of Frontier Interdisciplinary Fields (No. 1960523142).

References

[1] Zhang Y, Liu J, Li SL, et al. Polyoxometalate-based materials for sustainable and clean energy conversion and storage[J]. EnergyChem, 2019, 1: (3): 100021.

[2] Turner J A. Sustainable hydrogen production[J]. Science, 2004, 305: (5686): 972-974.

[3] Benson E E, Kubiak C P, Sathrum A J, et al. Electrocatalytic and homogeneous approaches to conversion of CO_2 to liquid fuels[J]. Chemical Society Reviews, 2009, 38: (1): 89-99.

[4] Fan W K, Tahir M. Recent advances on cobalt metal organic frameworks (MOFs) for photocatalytic CO_2 reduction to renewable energy and fuels: A review on current progress and future directions[J]. Energy Conversion and Management, 2022, 253: 115180.

[5] Ibhadon A O, Fitzpatrick P. Heterogeneous photocatalysis: Recent advances and applications[J]. Catalysts, 2013: 189-218.

[6] Chawla H, Chandra A, Ingole P P, et al. Recent advancements in enhancement of photocatalytic activity using bismuth-based metal oxides Bi_2MO_6 (M=W, Mo, Cr) for environmental remediation and clean energy production[J]. Journal of Industrial and Engineering Chemistry, 2021, 95: 1-15.

[7] Guo W, Guo T, Zhang Y, et al. Progress on simultaneous photocatalytic degradation of pollutants and production of clean energy: A review[J]. Chemosphere, 2023, 339: 139486.

[8] Sambyal S, Sharma R, Mandyal P, et al. Advancement in two-dimensional carbonaceous nanomaterials for photocatalytic water detoxification and energy conversion[J]. Journal of Environmental Chemical Engineering, 2023, 11: (2): 109517.

[9] Ge J, Zhang Y, Park S J, Recent advances in carbonaceous photocatalysts with enhanced photocatalytic performances: A mini review[J]. Materials, 2019, 12(12), 1976.

[10] Kandy M M. Carbon-based photocatalysts for enhanced photocatalytic reduction of CO_2 to solar fuels[J]. Sustainable Energy & Fuels, 2020, 4: (2): 469-484.

[11] Raza A, Altaf S, Ali S, et al. Recent advances in carbonaceous sustainable nanomaterials for wastewater treatments[J]. Sustainable Materials and Technologies, 2022, 32: e00406.

[12] Wang J, Yin S, Zhang Q, et al. Single-Atom Fe-N_4 sites promote the triplet-energy transfer process of g-C_3N_4 for the photooxidation[J]. Journal of Catalysis, 2021, 404: 89-95.

[13] Wang X, Zhou P, Zhou Q, et al. Tandem photocatalytic production of H_2O_2 and propylene oxide on 5-Bromoisatin modified carbon nitride[J]. Chemical Engineering Journal, 2023, 476: 146488.

[14] Zhang S, Liu H, Yu J, et al. Multi-functional flexible 2D carbon nanostructured networks[J]. Nature Communications, 2020, 11: (1): 5134.

[15] Armano A, Agnello S. Two-dimensional carbon: A review of synthesis methods, and electronic, optical, and vibrational properties of single-layer graphene[J]. Journal of Carbon Research, 2019, 5(4): 67.

[16] Ning H, Guo D, Wang X, et al. Efficient CO_2 electroreduction over N-doped hieratically porous carbon derived from petroleum pitch[J]. Journal of Energy Chemistry, 2021, 56: 113-120.

[17] Ramesh Reddy N, Bhargav U, Mamatha Kumari M, et al. Review on the interface engineering in the carbonaceous titania for the improved photocatalytic hydrogen production[J]. International Journal of Hydrogen Energy, 2020, 45: (13): 7584-7615.

[18] Patnaik S, Martha S, Acharya S, et al. An overview of the modification of g-C_3N_4 with high carbon containing materials for photocatalytic applications[J]. Inorganic Chemistry Frontiers, 2016, 3: (3): 336-347.

[19] Wang X, Pan Y, Ning H, et al. Hierarchically micro- and meso-porous Fe-N_4O-doped carbon as robust electrocatalyst for CO_2 reduction[J]. Applied Catalysis B: Environmental, 2020, 266: 118630.

[20] Shandilya P, Saini A K, Sharma R, et al. An overview of synthesis and photocatalytic application of carbon quantum dots-based nanocomposites[J]. Novel Applications of Carbon Based Nano-materials, 2022: 5-35.

[21] Li X, Shen R, Ma S, et al. Graphene-based heterojunction photocatalysts[J]. Applied Surface Science, 2018, 430: 53-107.

[22] Wang Z, Lin Z, Shen S, et al. Advances in designing heterojunction photocatalytic materials[J]. Chinese Journal of Catalysis, 2021, 42: (5): 710-730.

[23] Zhu Y, Wan T, Wen X, et al. Tunable type I and II heterojunction of CoO_x nanoparticles confined in g-C_3N_4 nanotubes for photocatalytic hydrogen production[J]. Applied Catalysis B: Environmental, 2019, 244: 814-822.

[24] Paramanik L, Reddy K H, Parida K M. An energy band compactable B-rGO/$PbTiO_3$ p–n junction: a highly dynamic and durable photocatalyst for enhanced photocatalytic H_2 evolution[J]. Nanoscale, 2019, 11: (46): 22328-22342.

[25] Liu L, Liu J, Yang W, et al. Constructing a Z-scheme $ZnIn_2S_4$-S/CNTs/RP nanocomposite with modulated energy band alignment for enhanced photocatalytic hydrogen evolution[J]. Journal of Colloid and Interface Science, 2022, 608: 482-492.

[26] Jin Z, Zhang L, Wang G, et al. Graphdiyne formed a novel CuI-GD/g-C_3N_4 S-scheme heterojunction composite for efficient photocatalytic hydrogen evolution[J]. Sustainable Energy & Fuels, 2020, 4: (10): 5088-5101.

[27] Mishra S, Acharya R. Recent updates in modification strategies for escalated performance of graphene/MFe_2O_4 heterostructured photocatalysts towards energy and environmental applications[J]. Journal of Alloys and Compounds, 2023, 960: 170576.

[28] Li W, Wang X, Li M, et al. Construction of Z-scheme and p-n heterostructure: Three-dimensional porous g-C_3N_4/graphene oxide-Ag/AgBr composite for high-efficient hydrogen evolution[J]. Applied Catalysis B: Environmental, 2020, 268: 118384.

[29] Liu J, Wei X, Sun W, et al. Fabrication of S-scheme CdS-g-C_3N_4-graphene aerogel heterojunction for enhanced visible light driven photocatalysis[J]. Environmental Research, 2021, 197: 111136.

[30] Li Y, Xia Z, Yang Q, et al. Review on g-C_3N_4-based S-scheme heterojunction photocatalysts[J]. Journal of Materials Science & Technology, 2022, 125: 128-144.

[31] Kou J, Lu C, Wang J, et al. Selectivity enhancement in heterogeneous photocatalytic transformations[J]. Chemical reviews, 2017, 117: (3): 1445-1514.

[32] Li X, Yang X, Xue H, et al. Metal-organic frameworks as a platform for clean energy applications[J]. EnergyChem, 2020, 2: (2): 100027.

[33] Wang H Z, Zhao Y Z, Yang Z X, et al. Oxygen-incorporated carbon nitride porous nanosheets for highly efficient photoelectrocatalytic CO_2 reduction to formate[J]. New Carbon Materials, 2022, 37: (6): 1135-1142.

[34] Yue C, Zhu L, Qiu Y, et al. Recent advances of plasmonic elemental Bi based photocatalysts in environmental remediation and energy conversion[J]. Journal of cleaner production, 2023, 392: 136017.

[35] Xu W, Zhao X, An X, et al. Alkali halide boost of carbon nitride for photocatalytic H_2 evolution in seawater[J]. ACS Applied Materials & Interfaces, 2020, 12: (43): 48526-48532.

[36] Ismael M. A review and recent advances in solar-to-hydrogen energy conversion based on photocatalytic water splitting over doped-TiO_2 nanoparticles[J]. Solar Energy, 2020, 211: 522-546.

[37] Marepally B C, Ampelli C, Genovese C, et al. Chapter 1 - Production of Solar Fuels Using CO_2 [M]. Studies in Surface Science and Catalysis, 2019: 7-30.

[38] Kumar A, Rana S, Sharma G, et al. Recent advances in zeolitic imidazole frameworks based photocatalysts for organic pollutant degradation and clean energy production[J]. Journal of Environmental Chemical Engineering, 2023, 11: (5): 110770.

[39] Hisatomi T, Kubota J, Domen K. Recent advances in semiconductors for photocatalytic and photoelectrochemical water splitting[J]. Chemical Society Reviews, 2014, 43: (22): 7520-7535.

[40] Rana S, Kumar A, Dhiman P, et al. Progress in graphdiyne and phosphorene based composites and heterostructures as new age materials for photocatalytic hydrogen evolution[J]. Fuel, 2024, 356: 129630.

[41] Kumar A, Rana S, Wang T, et al. Advances in S-scheme heterojunction semiconductor photocatalysts for CO_2 reduction, nitrogen fixation and NO_x degradation[J]. Materials Science in Semiconductor Processing, 2023, 168: 107869.

[42] Kumar A, Sharma P, Sharma G, et al. Recent progress in advanced strategies to enhance the photocatalytic performance of metal molybdates for H_2 production and CO_2 reduction[J]. Journal of Alloys and Compounds, 2024, 971: 172665.

[43] Ong W J, Putri L K, Mohamed A R. Rational design of carbon-based 2D nanostructures for enhanced photocatalytic CO_2 reduction: A dimensionality perspective[J]. Chemistry –A European Journal, 2020, 26: (44): 9710-9748.

[44] Rana S, Kumar A, Sharma G, et al. Recent advances in perovskite-based Z-scheme and S-scheme heterojunctions for photocatalytic CO_2 reduction[J]. Chemosphere, 2023, 339: 139765.

[45] Balakrishnan A, Gaware G J, Chinthala M. Heterojunction photocatalysts for the removal of nitrophenol: A systematic review[J]. Chemosphere, 2023, 310: 136853.

[46] Kumar A, Khan M, He J, et al. Recent developments and challenges in practical application of visible –light –driven TiO_2–based heterojunctions for PPCP degradation: A critical

review[J]. Water Research, 2020, 170: 115356.

[47] Li X, Yu Z, Shao L, et al. A novel strategy to construct a visible-light-driven Z-scheme (ZnAl-LDH with active phase/g-C_3N_4) heterojunction catalyst via polydopamine bridge (a similar "bridge" structure)[J]. Journal of Hazardous Materials, 2020, 386: 121650.

[48] Wen J, Xie J, Chen X, et al. A review on g-C_3N_4-based photocatalysts[J]. Applied Surface Science, 2017, 391: 72-123.

[49] Zhang X, Yuan X, Jiang L, et al. Powerful combination of 2D g-C_3N_4 and 2D nanomaterials for photocatalysis: Recent advances[J]. Chemical Engineering Journal, 2020, 390: 124475.

[50] Wen X J, Shen C H, Fei Z H, et al. Recent developments on AgI based heterojunction photocatalytic systems in photocatalytic application[J]. Chemical Engineering Journal, 2020, 383: 123083.

[51] Xu Q, Zhang L, Yu J, et al. Direct Z-scheme photocatalysts: Principles, synthesis and applications[J]. Materials Today, 2018, 21: (10): 1042-1063.

[52] Maeda K. Z-Scheme water splitting using two different semiconductor photocatalysts[J]. ACS Catalysis, 2013, 3: (7): 1486-1503.

[53] Xu Q, Zhang L, Cheng B, et al. S-scheme heterojunction photocatalyst[J]. Chem, 2020, 6: (7): 1543-1559.

[54] Zhou P, Yu J, Jaroniec M. All-solid-state Z-scheme photocatalytic systems[J]. Advanced Materials, 2014, 26: (29): 4920-4935.

[55] Low J, Dai B, Tong T, et al. In situ irradiated X-ray photoelectron spectroscopy investigation on a direct Z-scheme TiO_2/CdS composite film photocatalyst[J]. Advanced Materials, 2019, 31: (6): 1802981.

[56] Ani I, Akpan U, Olutoye M, et al. Photocatalytic degradation of pollutants in petroleum refinery wastewater by TiO_2-and ZnO-based photocatalysts: Recent development[J]. Journal of cleaner production, 2018, 205: 930-954.

[57] He X, Kai T, Ding P. Heterojunction photocatalysts for degradation of the tetracycline antibiotic: A review[J]. Environmental Chemistry Letters, 2021, 19: (6): 4563-4601.

[58] He F, Meng A, Cheng B, et al. Enhanced photocatalytic H_2-production activity of WO_3/TiO_2 step-scheme heterojunction by graphene modification[J]. Chinese Journal of Catalysis, 2020, 41: (1): 9-20.

[59] Mu J, Teng F, Miao H, et al. In-situ oxidation fabrication of 0D/2D SnO_2/SnS_2 novel Step-scheme heterojunctions with enhanced photoelectrochemical activity for water splitting[J]. Applied Surface Science, 2020, 501: 143974.

[60] Hu T, Dai K, Zhang J, et al. One-pot synthesis of step-scheme Bi_2S_3/porous g-C_3N_4 heterostructure for enhanced photocatalytic performance[J]. Materials Letters, 2019, 257: 126740.

[61] Bao Y, Song S, Yao G, et al. S-scheme photocatalytic systems[J]. Solar RRL, 2021, 5: (7): 2100118.

[62] Gaur M, Misra C, Yadav A B, et al. Biomedical applications of carbon nanomaterials: Fullerenes, quantum dots, nanotubes, nanofibers, and graphene[J]. Materials, 2021, 14: (20): 5978.

[63] Mohapatra L, Cheon D, Yoo S H. Carbon-based nanomaterials for catalytic wastewater treatment: A review[J]. Molecules, 2023, 28: (4): 1805.

[64] Huang W, Xiao S, Zhong H, et al. Activation of persulfates by carbon materials: A review[J]. Chemical Engineering Journal, 2021, 418: 129297.

[65] Leary R, Westwood A. Carbonaceous nanomaterials for the enhancement of TiO_2 photocatalysis[J]. Carbon, 2011, 49: (3): 741-772.

[66] Wang J, Lim Y F, Wei Ho G. Carbon-ensemble-manipulated ZnS heterostructures for enhanced photocatalytic H_2 evolution[J]. Nanoscale, 2014, 6: (16): 9673-9680.

[67] Xia G, Tian Y, Yin X, et al. Maximizing electrochemical hydrogen peroxide production from oxygen reduction with superaerophilic electrodes[J]. Applied Catalysis B: Environmental, 2021, 299: 120655.

[68] Li Y, Zhang H, Liu P, et al. Cross-Linked g-C_3N_4/rGO nanocomposites with tunable band structure and enhanced visible light photocatalytic activity[J]. Small, 2013, 9: (19): 3336-3344.

[69] Jahan S, Mansoor F, Naz S, et al. Oxidative synthesis of highly fluorescent boron/nitrogen co-doped carbon nanodots enabling detection of photosensitizer and carcinogenic dye[J]. Analytical Chemistry, 2013, 85: (21): 10232-10239.

[70] Tan X, Zhang J, Cao F, et al. Salt effect engineering single Fe-N_2P_2-Cl sites on interlinked porous carbon nanosheets for superior oxygen reduction reaction and Zn-air batteries[J]. Advanced Science, 2024, 11: (12): 2306599.

[71] Singla S, Sharma S, Basu S, et al. Photocatalytic water splitting hydrogen production via environmental benign carbon based nanomaterials[J]. International Journal of Hydrogen Energy, 2021, 46: (68): 33696-33717.

[72] Liang Q, Li Z, Huang Z H, et al. Holey graphitic carbon nitride nanosheets with carbon vacancies for highly improved photocatalytic hydrogen production[J]. Advanced Functional Materials, 2015, 25: (44): 6885-6892.

[73] Meng X, Dong Y, Hu Q, et al. Co Nanoparticles decorated with nitrogen doped carbon nanotubes for boosting photocatalytic water splitting[J]. ACS Sustainable Chemistry & Engineering, 2019, 7: (1): 1753-1759.

[74] Kang S-Z, Chen L, Li X, et al. Composite photocatalyst containing Eosin Y and multiwalled carbon nanotubes loaded with CuO/NiO: Mixed metal oxide as an active center of H_2 evolution from water[J]. Applied Surface Science, 2012, 258: (16): 6029-6033.

[75] Tasis D, Tagmatarchis N, Bianco A, et al. Chemistry of carbon nanotubes[J]. Chemical reviews, 2006, 106: (3): 1105-1136.

[76] De Jong K P, Geus J W. Carbon nanofibers: Catalytic synthesis and applications[J]. Catalysis Reviews, 2000, 42: (4): 481-510.

[77] Osorio-Aguilar D-M, Saldarriaga-Noreña H-A, Murillo-Tovar M-A, et al. Adsorption and photocatalytic degradation of methylene blue in carbon nanotubes: A review with bibliometric analysis[J]. Catalysts, 2023, 13: (12): 1480.

[78] Kuvarega A T, Mamba B B. TiO_2-based photocatalysis: Toward visible light-responsive photocatalysts through doping and

fabrication of carbon-based nanocomposites[J]. Critical Reviews in Solid State and Materials Sciences, 2017, 42: (4): 295-346.

[79] Farhadian M, Sangpour P, Hosseinzadeh G. Preparation and photocatalytic activity of WO_3–MWCNT nanocomposite for degradation of naphthalene under visible light irradiation[J]. RSC Advances, 2016, 6: (45): 39063-39073.

[80] Keshavarz S, Okoro O V, Hamidi M, et al. Synthesis, surface modifications, and biomedical applications of carbon nanofibers: Electrospun vs vapor-grown carbon nanofibers[J]. Coordination Chemistry Reviews, 2022, 472: 214770.

[81] Chung K H, Jeong S, Kim B J, et al. Enhancement of photocatalytic hydrogen production by liquid phase plasma irradiation on metal-loaded TiO_2/carbon nanofiber photocatalysts[J]. International Journal of Hydrogen Energy, 2018, 43: (24): 11422-11429.

[82] Wang X, Wang W, Zhang J, et al. Carbon sustained SnO_2-Bi_2O_3 hollow nanofibers as Janus catalyst for high-efficiency CO_2 electroreduction[J]. Chemical Engineering Journal, 2021, 426: 131867.

[83] Feng C, Chen Z, Jing J, et al. Significantly enhanced photocatalytic hydrogen production performance of g-C_3N_4/CNTs/CdZnS with carbon nanotubes as the electron mediators[J]. Journal of Materials Science & Technology, 2021, 80: 75-83.

[84] Xu Z, Shi W, Shi Y, et al. Carbon dots as solid-state electron mediator and electron acceptor in S-scheme heterojunction for boosted photocatalytic hydrogen evolution[J]. Applied Surface Science, 2022, 595: 153482.

[85] Shen L M, Liu J. New development in carbon quantum dots technical applications[J]. Talanta, 2016, 156-157: 245-256.

[86] Wu Y, Tang L, Liu D, et al. In-situ synthesis of high thermal stability and salt resistance carbon dots for injection pressure reduction and enhanced oil recovery[J]. Nano Research, 2023, 16: (10): 12058-12065.

[87] Sabet M, Mahdavi K. Green synthesis of high photoluminescence nitrogen-doped carbon quantum dots from grass via a simple hydrothermal method for removing organic and inorganic water pollutions[J]. Applied Surface Science, 2019, 463: 283-291.

[88] Mishra A, Basu S, Shetti N P, et al. Chapter 27-Photocatalysis of Graphene and Carbon Nitride-based Functional Carbon Quantum Dots[M]. Nanoscale Materials in Water Purification, 2019, 759-781.

[89] Heng Z W, Chong W C, Pang Y L, et al. An overview of the recent advances of carbon quantum dots/metal oxides in the application of heterogeneous photocatalysis in photodegradation of pollutants towards visible-light and solar energy exploitation[J]. Journal of Environmental Chemical Engineering, 2021, 9: (3): 105199.

[90] Wu X, Zhao Q, Zhang J, et al. 0D carbon dots intercalated Z-scheme CuO/g-C_3N_4 heterojunction with dual charge transfer pathways for synergetic visible-light-driven photo-Fenton-like catalysis[J]. Journal of Colloid and Interface Science, 2023, 634: 972-982.

[91] Wu X, Zhao Q, Guo F, et al. Porous g-C_3N_4 and α-FeOOH bridged by carbon dots as synergetic visible-light-driven photo-fenton catalysts for contaminated water remediation[J]. Carbon, 2021, 183: 628-640.

[92] Gao W, Zhang S, Wang G, et al. A review on mechanism, applications and influencing factors of carbon quantum dots based photocatalysis[J]. Ceramics International, 2022, 48: (24): 35986-35999.

[93] Bointon T H, Barnes M D, Russo S, et al. High quality monolayer graphene synthesized by resistive heating cold wall chemical vapor deposition[J]. Advanced Materials, 2015, 27: (28): 4200-4206.

[94] Wu X, Liu T, Ni W, et al. Engineering controllable oxygen vacancy defects in iron hydroxide oxide immobilized on reduced graphene oxide for boosting visible light-driven photo-Fenton-like oxidation[J]. Journal of Colloid and Interface Science, 2022, 623: 9-20.

[95] Qiu J, Zhang P, Ling M, et al. Photocatalytic synthesis of TiO_2 and reduced graphene oxide nanocomposite for lithium ion battery[J]. ACS Applied Materials & Interfaces, 2012, 4: (7): 3636-3642.

[96] Khan F, Khan M S, Kamal S, et al. Recent advances in graphene oxide and reduced graphene oxide based nanocomposites for the photodegradation of dyes[J]. Journal of Materials Chemistry C, 2020, 8: (45): 15940-15955.

[97] Gupta V K, Eren T, Atar N, et al. $CoFe_2O_4$@TiO_2 decorated reduced graphene oxide nanocomposite for photocatalytic degradation of chlorpyrifos[J]. Journal of Molecular Liquids, 2015, 208: 122-129.

[98] Shetti N P, Malode S J, Malladi R S, et al. Electrochemical detection and degradation of textile dye Congo red at graphene oxide modified electrode[J]. Microchemical Journal, 2019, 146: 387-392.

[99] Mohd Kaus N H, Rithwan A F, Adnan R, et al. Effective strategies, mechanisms, and photocatalytic efficiency of semiconductor nanomaterials incorporating rGO for environmental contaminant degradation[J]. Catalysts, 2021, 11: (3): 302.

[100] Dai H, Huang Y, Huang H. Eco-friendly polyvinyl alcohol/carboxymethyl cellulose hydrogels reinforced with graphene oxide and bentonite for enhanced adsorption of methylene blue[J]. Carbohydrate Polymers, 2018, 185: 1-11.

[101] Gebreegziabher G G, Asemahegne A S, Ayele D W, et al. One-step synthesis and characterization of reduced graphene oxide using chemical exfoliation method[J]. Materials Today Chemistry, 2019, 12: 233-239.

[102] Perveen M, Noreen L, Waqas M, et al. A DFT approach for finding therapeutic potential of graphyne as a nanocarrier in the doxorubicin drug delivery to treat cancer[J]. Journal of Molecular Graphics and Modelling, 2023, 124: 108537.

[103] Barua M, Saraswat A, Rao C N R. A novel method for synthesis of γ-graphyne and their charge transfer properties[J]. Carbon, 2022, 200: 247-252.

[104] Fan Z, Lu H, Liu Y, et al. Distinctive graphdiyne coupled with phosphorylation NiFe-LDH S-scheme heterojunction for photocatalytic overall water splitting[J]. Chemical Engineering Journal, 2023, 477: 147008.

[105] Gong Y, Shen L, Kang Z, et al. Progress in energy-related graphyne-based materials: Advanced synthesis, functional mechanisms and applications[J]. Journal of Materials Chemistry A, 2020, 8: (41): 21408-21433.

[106] Guo S, Jiang Y, Wu F, et al. Graphdiyne-promoted highly efficient photocatalytic activity of graphdiyne/silver phosphate pickering emulsion under visible-light irradiation[J]. ACS Applied Materials & Interfaces, 2019, 11: (3): 2684-2691.

[107] Yang C, Li Y, Chen Y, et al. Mechanochemical synthesis of γ-graphyne with enhanced lithium storage performance[J]. Small, 2019, 15: (8): 1804710.

[108] Baughman R H, Eckhardt H, Kertesz M. Structure-property predictions for new planar forms of carbon: Layered phases containing sp_2 and sp atoms[J]. The Journal of Chemical Physics, 1987, 87: (11): 6687-6699.

[109] Kang J, Li J, Wu F, et al. Elastic, Electronic, and optical properties of two-dimensional graphyne sheet[J]. The Journal of Physical Chemistry C, 2011, 115: (42): 20466-20470.

[110] Anafcheh M, Ektefa F. Cyclosulfurization of C_{60} and C_{70} fullerenes: A DFT study[J]. Structural Chemistry, 2015, 26: 1115-1124.

[111] Tycko R, Haddon R C, Dabbagh G, et al. Solid-state magnetic resonance spectroscopy of fullerenes[J]. The Journal of Physical Chemistry, 1991, 95: (2): 518-520.

[112] Pan Y, Liu X, Zhang W, et al. Advances in photocatalysis based on fullerene C_{60} and its derivatives: Properties, mechanism, synthesis, and applications[J]. Applied Catalysis B: Environmental, 2020, 265: 118579.

[113] Hasobe T, Imahori H, Fukuzumi S, et al. Light energy conversion using mixed molecular nanoclusters. Porphyrin and C_{60} cluster films for efficient photocurrent generation[J]. The Journal of Physical Chemistry B, 2003, 107: (44): 12105-12112.

[114] Long D, Chen W, Rao X, et al. Synergetic effect of C_{60}/g-C_3N_4 nanowire composites for enhanced photocatalytic H_2 evolution under visible light irradiation[J]. ChemCatChem, 2020, 12: (7): 2022-2031.

[115] Song L, Li T, Zhang S. Fullerenes/graphite carbon nitride with enhanced photocatalytic hydrogen evolution ability[J]. The Journal of Physical Chemistry C, 2017, 121: (1): 293-299.

[116] He Y-O, Fu Y-M, Meng X, et al. Enhanced visible light-driven CO_2 reduction activity induced by Z-scheme heterojunction photocatalyst C_{60}/TpPa (COF)[J]. Applied Catalysis A: General, 2023, 663: 119320.

[117] Ge J, Zhang Y, Park S-J. Recent Advances in carbonaceous photocatalysts with enhanced photocatalytic performances: A mini review[J]. Materials, 2019, 12: (12): 1916.

[118] Enterría M, Figueiredo J L. Nanostructured mesoporous carbons: Tuning texture and surface chemistry[J]. Carbon, 2016, 108: 79-102.

[119] Zhuo H, Hu Y, Tong X, et al. Sustainable hierarchical porous carbon aerogel from cellulose for high-performance supercapacitor and CO_2 capture[J]. Industrial Crops and Products, 2016, 87: 229-235.

[120] Gan G, Li X, Fan S, et al. Carbon aerogels for environmental clean-up[J]. European Journal of Inorganic Chemistry, 2019, 2019: (27): 3126-3141.

[121] Lee J-H, Park S-J. Recent advances in preparations and applications of carbon aerogels: A review[J]. Carbon, 2020, 163: 1-18.

[122] Liu Q, Cao J, Ji Y, et al. The direct Z-scheme $Cd_xZn_{1-x}S$ nanorods-Fe_2O_3 quantum dots heterojunction/reduced graphene oxide nanocomposites for photocatalytic degradation and photocatalytic hydrogen evolution[J]. Applied Surface Science, 2021, 570: 151085.

[123] Meng J, Chen Q, Lu J, et al. Z-Scheme photocatalytic CO_2 reduction on a heterostructure of oxygen-defective ZnO/reduced graphene oxide/UiO-66-NH_2 under visible light[J]. ACS Applied Materials & Interfaces, 2019, 11: (1): 550-562.

[124] Tian Z, Yang X, Chen Y, et al. Construction of $LaFeO_3$/g-C_3N_4 nanosheet-graphene heterojunction with built-in electric field for efficient visible-light photocatalytic hydrogen production[J]. Journal of Alloys and Compounds, 2022, 890: 161850.

[125] Deng W, Hao X, Shao Y, et al. Construction of 2D-2D S-scheme heterojunction based graphdiyne (g-C_nH_{2n-2}) coupling with highly crystalline nitrogen defect g-C_3N_4 for efficient photocatalytic overall water splitting[J]. Separation and Purification Technology, 2023, 323: 124375.

[126] Wang B, Zhao J, Chen H, et al. Unique Z-scheme carbonized polymer dots/$Bi_4O_5Br_2$ hybrids for efficiently boosting photocatalytic CO_2 reduction[J]. Applied Catalysis B: Environmental, 2021, 293: 120182.

[127] Bafaqeer A, Tahir M, Amin N A S, et al. Performance analysis of rGO-bridged g-C_3N_4/ZnV_2O_6 S-scheme heterojunction for CO_2 photoreduction with H_2O in an externally reflected photoreactor[J]. Journal of Alloys and Compounds, 2023, 968: 171833.

[128] Balapure A, Dutta J R, Ganesan R. Recent advances in semiconductor heterojunction: A detailed review of fundamentals of the photocatalysis, charge transfer mechanism, and materials[J]. RSC Applied Interfaces, 2023.

[129] Sharma K, Hasija V, Malhotra M, et al. A review of CdS-based S-scheme for photocatalytic water splitting: Synthetic strategy and identification techniques[J]. International Journal of Hydrogen Energy, 2024, 52: 804-818.

[130] Liu Y, Shang J, Zhu T. Enhanced thermal-assisted photocatalytic CO_2 reduction by RGO/H-CN two-dimensional heterojunction[J]. Journal of Materials Science & Technology, 2024, 176: 36-47.

[131] Guo X, Xiao Q, Yang T, et al. Construction of S-Scheme Co_2SnO_4/graphdiyne heterojunction to promote carrier transfer for efficiently photocatalytic hydrogen evolution characterized with in

situ XPS[J]. Separation and Purification Technology, 2023, 325: 124764.

[132] Yang X, Sheng L, Ye Y, et al. Recent advances in metal-free CDs/g-C_3N_4 photocatalysts: Synthetic strategies, mechanism insight, and applications[J]. Journal of Materials Science & Technology, 2023, 150: 11-26.

[133] Velempini T, Prabakaran E, Pillay K. Recent developments in the use of metal oxides for photocatalytic degradation of pharmaceutical pollutants in water—a review[J]. Materials Today Chemistry, 2021, 19: 100380.

[134] Dutta V, Sharma S, Raizada P, et al. An overview on WO_3 based photocatalyst for environmental remediation[J]. Journal of Environmental Chemical Engineering, 2021, 9: (1): 105018.

[135] Ismael M. Ferrites as solar photocatalytic materials and their activities in solar energy conversion and environmental protection: A review[J]. Solar Energy Materials and Solar Cells, 2021, 219: 110786.

[136] Liu Y, Shen S, Li Z, et al. Mesoporous g-C_3N_4 nanosheets with improved photocatalytic performance for hydrogen evolution[J]. Materials Characterization, 2021, 174: 111031.

[137] Shandilya P, Sambyal S, Sharma R, et al. Properties, optimized morphologies, and advanced strategies for photocatalytic applications of WO_3 based photocatalysts[J]. Journal of Hazardous Materials, 2022, 428: 128218.

[138] Jin Z, Wang T, Cui E, et al. Constructing a tandem heterojunction: S-scheme heterojunction and Ohmic junction based on graphdiyne, synergistically optimizing photocatalytic hydrogen evolution[J]. Chemical Engineering Journal, 2023, 477: 147210.

[139] Alharthi F A, Ababtain A S, Alanazi H S, et al. Zinc vanadate ($Zn_3V_2O_8$) immobilized multiwall carbon nanotube (MWCNT) heterojunction as an efficient photocatalyst for visible light driven hydrogen production[J]. Molecules, 2023, 28: (3): 1362.

[140] Jiao Y, Huang Q, Wang J, et al. A novel MoS_2 quantum dots (QDs) decorated Z-scheme g-C_3N_4 nanosheet/N-doped carbon dots heterostructure photocatalyst for photocatalytic hydrogen evolution[J]. Applied Catalysis B: Environmental, 2019, 247: 124-132.

[141] Hu Z, Shi D, Wang G, et al. Carbon dots incorporated in hierarchical macro/mesoporous g-C_3N_4/TiO_2 as an all-solid-state Z-scheme heterojunction for enhancement of photocatalytic H_2 evolution under visible light[J]. Applied Surface Science, 2022, 601: 154167.

[142] Jiao Y, Li Y, Wang J, et al. Exfoliation-induced exposure of active sites for g-C_3N_4/N-doped carbon dots heterojunction to improve hydrogen evolution activity[J]. Molecular Catalysis, 2020, 497: 111223.

[143] Song T, Zhang X, Yang P. Bifunctional nitrogen-doped carbon dots in g-C_3N_4/WO_x heterojunction for enhanced photocatalytic water-splitting performance[J]. Langmuir, 2021, 37: (14): 4236-4247.

[144] Jiao Y, Li Y, Wang J, et al. Double Z-scheme photocatalyst C_3N_4 nanotube/N-doped carbon dots/Ni_2P with enhanced visible-light photocatalytic activity for hydrogen generation[J]. Applied Surface Science, 2020, 534: 147603.

[145] Shang Y, Liu T, Chen G, et al. N, P co-doped carbon quantum dots bridge g-C_3N_4 and SnO_2: Accelerating charge transport in S-scheme heterojunction for enhanced photocatalytic hydrogen production[J]. Journal of Alloys and Compounds, 2024, 971: 172667.

[146] Li X, Luo Q, Han L, et al. Enhanced photocatalytic degradation and H_2 evolution performance of NCDs/S-C_3N_4 S-scheme heterojunction constructed by π-π conjugate self-assembly[J]. Journal of Materials Science & Technology, 2022, 114: 222-232.

[147] Xue W, Hu X, Liu E, et al. Novel reduced graphene oxide-supported $Cd_{0.5}Zn_{0.5}S$/g-C_3N_4 Z-scheme heterojunction photocatalyst for enhanced hydrogen evolution[J]. Applied Surface Science, 2018, 447: 783-794.

[148] Galal A H, Elmahgary M G, Ahmed M A. Construction of novel $AgIO_4$/ZnO/graphene direct Z-scheme heterojunctions for exceptional photocatalytic hydrogen gas production[J]. Nanotechnology for Environmental Engineering, 2021, 6: (1): 5.

[149] Lv T, Wang H, Hong W, et al. In situ self-assembly synthesis of sandwich-like TiO_2/reduced graphene oxide/$LaFeO_3$ Z-scheme ternary heterostructure towards enhanced photocatalytic hydrogen production[J]. Molecular Catalysis, 2019, 475: 110497.

[150] Raja A, Son N, Kang M. Direct Z-scheme $ZnIn_2S_4$ spheres and CeO_2 nanorods decorated on reduced-graphene-oxide heterojunction photocatalysts for hydrogen evolution and photocatalytic degradation[J]. Applied Surface Science, 2023, 607: 155087.

[151] Shaheer A R M, Vinesh V, Lakhera S K, et al. Reduced graphene oxide as a solid-state mediator in TiO_2/$In_{0.5}WO_3$ S-scheme photocatalyst for hydrogen production[J]. Solar Energy, 2021, 213: 260-270.

[152] Liang S, Wang J, Lin Q, et al. Interface-optimized Rh-ZnO/rGO/ZnS heterostructure constructed via Rh-induced dynamic micro-cell growth for efficient photocatalytic hydrogen evolution[J]. Journal of Alloys and Compounds, 2022, 904: 164021.

[153] Belakehal R, Güy N, Atacan K, et al. Emerging n-p-n $Mn_{0.2}Cd_{0.8}S$/$CoFe_2O_4$/rGO S-scheme heterojunction for synergistically improved photocatalytic H_2 production[J]. Materials Chemistry and Physics, 2023, 310: 128453.

[154] Samajdar S, Bera S, Das P S, et al. Exploration of 1D-2D $LaFeO_3$/RGO S-scheme heterojunction for photocatalytic water splitting[J]. International Journal of Hydrogen Energy, 2023, 48: (47): 17838-17851.

[155] Ibrahim Y O, Hezam A, Qahtan T F, et al. Laser-assisted synthesis of Z-scheme TiO_2/rGO/g-C_3N_4 nanocomposites for highly enhanced photocatalytic hydrogen evolution[J]. Applied Surface Science, 2020, 534: 147578.

[156] Park H, Son N, Park B H, et al. Switching of a type I to an all-solid-state Z-scheme heterojunction by an electron mediator rGO bridge:18.4% solar-to-hydrogen efficiency in n-ZnS/rGO/p-Bi_2S_3

ternary catalyst[J]. Chemical Engineering Journal, 2022, 430: 133104.

[157] Sarkar A, Mandal M K, Das S, et al. Facile in-situ synthesis of solid mediator based CdS-rGO-WO_3 Z-scheme photocatalytic system for efficient photocatalytic hydrogen generation[J]. Optical Materials, 2024, 147: 114670.

[158] Li T, Jin Z. Rationally engineered avtive sites for efficient and durable hydrogen production over γ-graphyne assembly $CuMoO_4$ S-scheme heterojunction[J]. Journal of Catalysis, 2023, 417: 274-285.

[159] Jin Z, Wu Y. Novel preparation strategy of graphdiyne (C_nH_{2n-2}): One-pot conjugation and S-Scheme heterojunctions formed with MoP characterized with in situ XPS for efficiently photocatalytic hydrogen evolution[J]. Applied Catalysis B: Environmental, 2023, 327: 122461.

[160] Li X, Lei M, Jin Z. Reinforced photogenerated electrons transfer on a novel graphdiyne(C_nH_{2n-2}) based heterojunction for enhanced photocatalytic hydrogen production[J]. Journal of Catalysis, 2023, 428: 115131.

[161] Wang T, Jin Z. Graphdiyne (C_nH_{2n-2}) based CuI-GDY/ZnAl LDH double S-scheme heterojunction proved with in situ XPS for efficient photocatalytic hydrogen production[J]. Journal of Materials Science & Technology, 2023, 155: 132-141.

[162] Li T, Wang X, Jin Z, et al. Enhanced kinetics of photocatalytic hydrogen evolution by interfacial Co-C bonded strongly coupled S-scheme inorganic perovskite/organic graphdiyne (CnH_{2n-2}) heterojunction[J]. Chemical Engineering Journal, 2023, 477: 147018.

[163] Liu H, Sun F, Li X, et al. g-C_3N_4/TiO_2/$ZnIn_2S_4$ graphene aerogel photocatalysts with double S-scheme heterostructure for improving photocatalytic multifunctional performances[J]. Composites Part B: Engineering, 2023, 259: 110746.

[164] Balan B, Xavier M M, Mathew S. MoS_2-based nanocomposites for photocatalytic hydrogen evolution and carbon dioxide reduction[J]. ACS Omega, 2023, 8: (29): 25649-25673.

[165] Deng X, Liu C, Yan X, et al. Carbon dots anchored NiAl-LDH@In_2O_3 hierarchical nanotubes for promoting selective CO_2 photoreduction into CH_4[J]. Chinese Chemical Letters, 2023, 35(6), 108942.

[166] Li X, Guan J, Jiang H, et al. rGO modified R-CeO_2/g-C_3N_4 multi-interface contact S-scheme photocatalyst for efficient CO_2 photoreduction[J]. Applied Surface Science, 2021, 563: 150042.

[167] Kong X, Fan J, Feng B, et al. Carbon dots-triggered the fabrication of miniature g-C_3N_4/CDs/WO_3 S-scheme heterojunction for efficient CO_2 photoreduction[J]. Chemical Engineering Journal, 2023, 476: 146774.

[168] Guo R T, Bi Z X, Lin Z D, et al. Carbon quantum dots-modified Z-scheme $Bi_{12}O_{17}Cl_2$/NiAl-LDH for significantly boosting photocatalytic CO_2 reduction[J]. Journal of Colloid and Interface Science, 2022, 627: 343-354.

[169] Quan Y, Wang B, Liu G, et al. Carbonized polymer dots modified ultrathin $Bi_{12}O_{17}Cl_2$ nanosheets Z-scheme heterojunction for robust CO_2 photoreduction[J]. Chemical Engineering Science, 2021, 232: 116338.

[170] Xu D, Cheng B, Wang W, et al. Ag_2CrO_4/g-C_3N_4/graphene oxide ternary nanocomposite Z-scheme photocatalyst with enhanced CO_2 reduction activity[J]. Applied Catalysis B: Environmental, 2018, 231: 368-380.

[171] Luo Y, Han H, Zhang G, et al. Construction of Z-scheme α-Fe_2O_3/graphene/Bi_2O_2S heterojunction for visible-light-driven photocatalytic CO_2 conversion[J]. Separation and Purification Technology, 2023, 314: 123607.

[172] Wang P, Yang M, Tang S, et al. Z-scheme heterojunctions composed of 3D graphene aerogel/g-C_3N_4 nanosheets/porous ZnO nanospheres for the efficient photocatalytic reduction of CO_2 with H_2O under visible light irradiation[J]. Journal of Alloys and Compounds, 2022, 918: 165607.

[173] Hu X, Hu J, Peng Q, et al. Construction of 2D all-solid-state Z-scheme g-C_3N_4/BiOI/RGO hybrid structure immobilized on Ni foam for CO_2 reduction and pollutant degradation[J]. Materials Research Bulletin, 2020, 122: 110682.

[174] Jiang Y, Liao J F, Chen H Y, et al. All-solid-state Z-scheme α-Fe_2O_3/amine-RGO/$CsPbBr_3$ hybrids for visible-light-driven photocatalytic CO_2 reduction[J]. Chem, 2020, 6: (3): 766-780.

[175] Yin S, Li J, Sun L, et al. Construction of Heterogenous S–C–S MoS_2/SnS_2/r-GO Heterojunction for Efficient CO_2 Photoreduction[J]. Inorganic Chemistry, 2019, 58(22): 15590-15601.

[176] Bafaqeer A, Tahir M, Amin N A S, et al. Fabricating 2D/2D/2D heterojunction of graphene oxide mediated g-C_3N_4 and ZnV_2O_6 composite with kinetic modelling for photocatalytic CO2 reduction to fuels under UV and visible light[J]. Journal of Materials Science, 2021, 56(16): 9985-10007.

[177] Mu Y F, Zhang W, Dong G X, et al. Ultrathin and small-size graphene oxide as an electron mediator for perovskite-based Z-scheme system to significantly enhance photocatalytic CO_2 reduction[J]. Small, 2020, 16(29): 2002140.

[178] Bafaqeer A, Tahir M, Ali Khan A, et al. Indirect Z-Scheme assembly of 2D ZnV_2O_6/RGO/g-C_3N_4 nanosheets with RGO/pCN as solid-state electron mediators toward visible-light-enhanced CO_2 reduction[J]. Industrial & Engineering Chemistry Research, 2019, 58(20): 8612-8624.

[179] Kumar A, Prajapati P K, Pal U, et al. Ternary rGO/$InVO_4$/Fe_2O_3 Z-Scheme heterostructured photocatalyst for CO_2 reduction under visible light irradiation[J]. ACS Sustainable Chemistry & Engineering, 2018, 6(7): 8201-8211.

[180] Ikreedeegh R R, Tahir M. Indirect Z-scheme heterojunction of NH_2-MIL-125(Ti) MOF/g-C_3N_4 nanocomposite with RGO solid electron mediator for efficient photocatalytic CO_2 reduction to CO and CH_4[J]. Journal of Environmental Chemical Engineering, 2019, 9(4): 105600.

[181] Jo W-K, Kumar S, Eslava S, et al. Construction of Bi_2WO_6/RGO/g-C_3N_4 2D/2D/2D hybrid Z-scheme heterojunctions with large interfacial contact area for efficient charge separation

and high-performance photoreduction of CO_2 and H_2O into solar fuels[J]. Applied Catalysis B: Environmental, 2018, 239: 586-598.

[182] Wei J, Liang T, Zhang S, et al. Accelerated interfacial charges migration on Z-scheme CoAl-LDH/RGO/$InVO_4$ heterojunction for photocatalytic reduction of CO_2[J]. Separation and Purification Technology, 2023, 325: 124683.

[183] Yang Y, Wu J, Xiao T, et al. Urchin-like hierarchical CoZnAl-LDH/RGO/g-C_3N_4 hybrid as a Z-scheme photocatalyst for efficient and selective CO_2 reduction[J]. Applied Catalysis B: Environmental, 2019, 255: 117771.

[184] Gao M, Sun L, Ma C, et al. Constructed Z-Scheme g-C_3N_4/Ag_3VO_4/rGO photocatalysts with multi-interfacial electron-transfer paths for high photoreduction of CO_2[J]. Inorganic Chemistry, 2021, 60: (3): 1755-1766.

[185] Wu W, Bi H, Zhang Z, et al. Z-scheme π-π stacking MXene/GO/PDI composite aerogels to construct interface electron transport network for photocatalytic CO_2 reduction[J]. Colloids and Surfaces A: Physicochemical and Engineering Aspects, 2023, 657: 130486.

[186] Shi Z-J, Ma M-G, Zhu J-F. Recent development of photocatalysts containing carbon species: A review[J]. Catalysts, 2019, 9: (1): 20.

[187] Liu Z, Ling Q, Cai Y, et al. Synthesis of carbon-based nanomaterials and their application in pollution management[J]. 2022, 4: (5): 1246-1262.

[188] Gong E, Ali S, Hiragond C B, et al. Solar fuels: Research and development strategies to accelerate photocatalytic CO_2 conversion into hydrocarbon fuels[J]. Energy & Environmental Science, 2022, 15: (3): 880-937.

[189] Ge J, Zhang Y, Park S J. Recent advances in carbonaceous photocatalysts with enhanced photocatalytic performances: A mini review[J]. Materials (Basel), 2019, 12(12): 1916.